Reduced Order Modeling of Reactor Pressure Vessels for Probabilistic Fracture Mechanics

A Thesis

Presented in Partial Fulfillment of the Requirements for the

Degree of Master of Science

with a

Major in Mechanical Engineering

in the

College of Graduate Studies

University of Idaho

by

William M. Hoffman

Major Professor: Matthew Riley, Ph.D.

Committee Members: Matthew Riley, Ph.D.;

Gabriel Potirniche, Ph.D.; Robert Stephens, Ph.D.

Department Administrator: Steven Beyerlein, Ph.D.

May 2016

Authorization to Submit Thesis

This thesis of William M. Hoffman, submitted for the degree of Master of Science with a Major in Mechanical Engineering and titled "Reduced Order Modeling of Reactor Pressure Vessels for Probabilistic Fracture Mechanics," has been reviewed in final form. Permission, as indicated by the signatures and dates given below, is now granted to submit final copies to the College of Graduate Studies for Approval.

Major Professor: _____ Date: _____
Matthew Riley, Ph.D.

Committee Members: _____ Date: _____
Gabriel Potirniche, Ph.D.

_____ Date: _____
Robert Stephens, Ph.D.

Department Administrator: _____ Date: _____
Steven Beyerlein, Ph.D.

Abstract

In order to provide efficient estimates on the safe life of damaged nuclear Reactor Pressure Vessels (RPVs), simulation based models have been created for probabilistic analyses. As probabilistic analyses generally require millions of model evaluations, a model for rapid and accurate stress intensity factor calculations is necessary to obtain useful stochastic results. The Fracture Analysis of Vessels, FAVOR code, is a program designed to perform probabilistic assessments of RPVs, though its analysis is limited to axis aligned flaws for discrete flaw characteristic inputs. In an effort to extend this analysis to 3D off axis flaws for any continuous input, the weight function method utilized in FAVOR was implemented within a finite element framework more conducive to 3D flaw evaluations. Using the INL's fracture mechanics and material embrittlement code, Grizzly, RPV fracture models were utilized in the development of a reduced order model for approximating stress intensity factors to enable efficient probabilistic analyses. Additionally, surrogate modeling techniques were investigated and utilized within the reduced order model such that continuous flaw inputs could be evaluated.

Table of Contents

List of Abbreviations

BWR – Boiling Water Reactor

FAVOR – Fracture Analysis of Vessels Oak Ridge

FEA – Finite Element Analysis

INL – Idaho National Laboratory

LSRSM – Least Squares Response Surface Methodology

LWR – Light Water Reactor

MOOSE – Multiphysics Object Oriented Simulation Environment

NRC – Nuclear Regulatory Commission

ORNL – Oak Ridge National Laboratory

PTS – Pressurized Thermal Shock

PWR – Pressurized Water Reactor

RPV – Reactor Pressure Vessel

SIFIC – Stress Intensity Factor Influence Coefficient

List of Figures

List of Tables

Chapter 1. Introduction

In nuclear power systems, specifically Light Water Reactor (LWR) systems, the reactor coolant, core and shroud are contained within a large, thick walled steel vessel known as a reactor pressure vessel (RPV) shown in Figure 1.1.

Figure 1.1: Reactor Pressure Vessel

RPVs can stand up to 12 meters tall with inner diameters on the order of five meters. They are commonly used in LWR systems as a means to contain not only the core of the reactor, but the large amount of water within the system used for both cooling and neutron moderation. LWR pressure vessels are required to safely contain water at temperatures up to 300˚C and internal pressures ranging from roughly 7-20MPa [1].

This work focuses on RPVs used in Pressurized Water Reactor (PWR) systems, which consist of two primary materials—the base metal and a relatively thin layer of

cladding. The base material is the outer wall of low alloy ferritic steel, with a thickness of approximately 15-20 centimeters. The cladding is the inner layer of austenitic stainless steel, often less than one centimeter thick, which lines the inner surface of the vessel to protect against corrosion [2]. Given the tremendous size of these structures and challenges within the manufacturing process, many RPVs contain a relatively high number of internal and surface defects from the day they are commissioned [3]. These flaws are typically of little concern in the early stages of a reactor's operating life as the vessel's constituent materials are ductile and thick. However, as the reactor operates, the neutrons emitted from the fuel within the vessel bombard the RPV steel. Over many years of operation, high levels of irradiation begin to change the material's behavior from ductile to brittle. [4]

Material aging and embrittlement, coupled with the cyclic and unpredictable nature of the pressure and thermal conditions within the RPV, result in a vessel wall that is particularly susceptible to crack nucleation and propagation. The RPV, which was commissioned with a potentially large population of flaws, becomes increasingly vulnerable to through wall cracking after many years of normal operation, where flaws are subject to fatigue conditions due to temperature and pressure oscillations. Therefore, assessing the safe life of these structures relies heavily on the material's damage tolerance. Damage tolerant systems such as cracked RPVs begin to require extra attention as they reach what is presumed to be the end of their safe operation periods. Regular and frequent inspections can help to identify large flaws or an overwhelming presence of flaws, but are inefficient and costly due to the requirement of removing that particular vessel from operation for service. More importantly, inspections provide little insight into how an RPV with several flaws may react to an abnormal event, and would likely require conservative operation period estimations in order to reduce the risk

of system failures. As such, simulation based studies are essential in assessing the risk associated with the continued operation of the RPVs [4].

For risk analysis, it is important to identify scenarios in which the risk of failure is greatest. For example, the normal operating conditions of the RPVs are very small contributors to the overall probability of through wall cracking, and although it is very important to look at all scenarios, they are not the focus of this particular research study. Instead, the scenario being evaluated is one which provides a large contribution to the overall probability of through wall cracking. This scenario is called a pressurized thermal shock (PTS) event [5]. A PTS event occurs when the RPV is subject to a rapid temperature change, or thermal shock, in addition to a significant existing or sudden internal pressure. The sharp thermal gradient in the vessel wall accompanied by a large mechanical load results in high thermal and mechanical stresses [6], conditions which are particularly conducive to rapid crack growth.

There are many different combinations of events that can lead to a pressurized thermal shock. For example, an RPV could experience a period where the system briefly loses cooling, eventually resulting in an abrupt re-cooling of the pressurized system. Another example could be a scenario where a pressure release valve suddenly closes during a cooling period, resulting in a sharp pressure increase. The particular event used in this study will be explained in greater detail in chapter 2.3.

There are several methods that can be used to measure an RPV's response to a PTS event, ranging from experimental tests or physical inspections over time to purely analytical methods [1] [7]. One method that has become increasingly prevalent is finite element analysis (FEA). In particular, FEA can be used to conduct a transient analysis of an RPV wall

which contains a flaw, or even multiple flaws. This is done by creating and applying time dependent model boundary conditions representative of the PTS event. Material properties and flaw characteristics are added to the model and it is evaluated, resulting in a deterministic value for the stress intensity factor of the flaw over time. In fracture mechanics, the stress intensity factor is used to predict the stress intensity at the tip of a crack or flaw. It is often denoted as K, and can be compared to the material's fracture toughness to predict whether or not the crack will propagate [8]. If the model output shows that the fracture toughness is less than the maximum value of the stress intensity factor, the module concludes that crack growth will occur, though details regarding its propagation would still be unknown.

A purely deterministic result, such as the outcome stated above, can be useful in many ways and in general provides a solid estimate of the outcome. However, this type of model does not account for any randomness within the system, and will by definition produce the same exact result until something about the model is changed. The potential issue with this result is that in reality, there is always some level of uncertainty that exists within these systems. Though it is generally not critical to incorporate every source of randomness into the model, it is important to at least identify large sources of randomness, and incorporate them if possible. This is especially important when making predictions involved in safety assessments.

For embrittled RPVs, a large amount of randomness exists within the flaw population. That is, at any given time, an RPV can contain a potentially large population of flaws with some distribution of sizes, shapes, and orientations. [9] The size of the population and variation of the flaw characteristics within the population are estimated and constantly changing. Therefore, a probabilistic approach that addresses the uncertainty within the flaw

population is more appropriate and would ultimately produce a more valuable result.

To achieve this, one approach would be to utilize the deterministic output from single flaw FEA models in order to conduct Monte Carlo analyses. In a Monte Carlo simulation, a deterministic model is evaluated numerous times, where input parameters are varied in a statistically predetermined way such that the large number of outputs forms a distribution, thus turning a deterministic model into a stochastic model. This particular method is valid and would provide adequate results, but is also extremely inefficient and computationally expensive. Single flaw evaluations using FEA packages such as MOOSE or Abaqus can require several minutes of computing time, and a full scale transient finite element analysis of a 3D RPV could potentially take days of computation time. Probabilistic assessment methods such as Monte Carlo simulations generally require the function of interest, in this case, an FEA flaw model, to be evaluated millions of times. This is generally infeasible for flaw models because individual model evaluations require too much computation time. For that reason, a method for the precise and rapid evaluation of the stress intensity factor for various flaws would be incredibly valuable. Such a process is often referred to as model order reduction, where a simpler reduced order model is created to stand in for the more complex and time consuming model. However, such a model would need to come at a minimal reduction in accuracy and must be significantly faster than the alternative in order to be truly useful in probabilistic analyses.

The desire for probability based RPV fracture models has been around for many years, prompting some research groups within the scientific community to develop programs to run probabilistic risk assessments on RPVs. One such program that is widely used in the literature [10] is called Fracture Analysis of Vessels – Oak Ridge (FAVOR). FAVOR is a

program developed by Oak Ridge National Lab that performs deterministic and probabilistic analyses of the structural integrity of an RPV when subjected to a range of thermal-hydraulic events. [11] Currently, FAVOR's analysis is focused solely on the beltline region of the RPV--the large unobstructed cylindrical wall of the RPV directly in-line with the fuel. This region of the RPV experiences the highest level of irradiation and is therefore the section most susceptible to embrittlement and, in general, also contains a large population of flaws. FAVOR's analysis is carried out, in part, by evaluating a 1D axisymmetric finite element model of the un-cracked RPV wall, in addition to utilizing a library of Stress Intensity Factor Influence Coefficients (SIFICs) that were generated for flaws aligned with the major axes of the RPV. FAVOR's method will be discussed in great detail in section 2.2.

While the methods utilized in FAVOR are sound, and the process is efficient, the analysis is limited to flaws aligned with the axes of the RPV, meaning axial or circumferential flaws subject to mode one loading from the hoop and axial stress in the vessel wall, respectively. Although this analysis is able to capture, in a sense, the worst case scenario [12], as the axial and hoop stresses in the vessel wall are the principal stresses and will have the largest effect on crack opening, the limitation lies in the fact that RPV is not fully and accurately portrayed. The probability of all flaws in the vessel being axial or circumferential is very low. Furthermore, because the eventual goal of this study is analyze the entire RPV's response, it would be beneficial to include off axis flaws. The development of a reduced order model for 3D off axis flaws would allow analyses to be extended to regions of the RPV beyond the belt-line, allowing for simulations in which the entire RPV can be assessed.

The overall goal of this research is to increase the effectiveness of current methods used for reliability analyses of RPVs subject to pressurized thermal shocks. Thus, the process of extending the methodology utilized in the FAVOR code, to accommodate off axis flaws, must be investigated. If off axis flaws can be evaluated in an efficient and accurate way, probabilistic assessments can be expanded to include more flaws in arbitrary orientations which would allow the analysis to be extended to regions beyond the RPV belt line. In order to accomplish this, the primary task and main focus of this work is to, in a sense, recreate FAVOR's deterministic flaw analysis in an environment that would enable 3D analysis. The department of Fuels Modeling and Simulation at the Idaho National Lab (INL) is currently developing a finite element based code called Grizzly in order to evaluate the structural integrity of embrittled RPV steel when subjected to off-normal operating conditions [13]. Additionally, new methods for interpolation between flaw characteristics and orientations will be investigated and implemented, as the method utilized in FAVOR would become a significant limitation in the transition to 3D off axis flaws.

The structure of this thesis will be as follows: Chapter 2 presents some of the relevant methods currently in use for the analysis of flaws in RPVs. Section 2.1 provides a detailed overview of the weight function method commonly used for RPV fracture analyses. Section 2.2, gives an in depth summary of the methods and framework used within FAVOR, as well as a discussion regarding its current applications and limitations. Then, in section 2.3, a detailed analysis and application of the INL's Grizzly code is presented. Chapter 3 then discusses the various surrogate modeling techniques which were investigated in order to approximate SIFICs as a function of flaw characteristics. Sections 3.1, 3.2, and 3.3 will provide detailed descriptions of the theory and application of interpolation, response surface

methodology, and ordinary kriging methods, respectively. Section 3.4 will present a study conducted in order to compare the different modeling techniques as well as its results. Chapter 4 will present the vision for the final analysis framework of the project. Within this chapter, the current implementation and results will be presented as well as plans for future implementation. Then, in Chapter 5, a summary of the major concepts as well as their application and results will be provided to conclude this thesis.

Chapter 2. RPV Analysis

In 1955, the United States took part in the largest gathering of scientists and engineers of that time in an event now known as "The First Geneva Convention." This gathering helped to absolve the post-war secrecy associated with nuclear research and helped to initiate the spread of nuclear power research. The United States placed a heavy emphasis on the development of Light Water Reactors (LWRs) which includes the subclasses of Pressurized Water Reactors (PWRs) and Boiling Water Reactors (BWRs), both of which initially spread quite rapidly throughout the US. The growth of the nuclear power industry quickly came to a halt after the accident at Three Mile Island on March 28th, 1979, as the meltdown had a significant effect on the public's opinion regarding the safety of these plans [14]. The incident largely ended the growth in new construction of nuclear power plants in the US, however, there remains a significant number of LWRs in use to this day.

For the reasons stated above, many of the RPVs currently in use have been for 50 years or more and have become heavily irradiated, a process which embrittles the RPV steel, making it particularly susceptible to fracture. RPV steels are required by the Nuclear Regulatory Commission (NRC) to maintain a conservative margin for fracture toughness, in order to safely contain the reactor in normal and off-normal events such as pressurized thermal shocks. As plants request license extensions for 60 or 80 years, there is very little data, if any, to aid in the safe life estimation of these vessels. This is largely due to the fact that most RPVs simply have not been in use for such a period. [15]

Therefore, the need for simulation based studies has become the focus of many research groups in an effort to extend PWR operations to 80 years or more. While there are many components within a PWR that are analyzed and inspected for license extension, the

most critical is the RPV which contains the entire assembly. Of particular interest in these evaluations is the embrittled and flawed RPV's response to pressurized thermal shock events. Thus, there has been a significant effort made over the past several years to develop simulation based methods in order to address this issue. This chapter will focus on the investigation and application of simulation based methods for analyzing RPVs and RPV flaws during PTS events.

2.1 The Weight Function Method

A key method that is often used to evaluate surface breaking elliptical flaws in RPVs uses a weight function in combination with the principle of linear superposition, a concept which is used in many physics and engineering applications. It states that the response of any linear system, when subject to two or more stimuli, is equal to the sum of the responses when each stimulus is considered individually. It was initially shown by Buckner [7], under the assumption of Linear Elastic Fracture Mechanics, that this principle could be applied to fracture models such that when combined with a weight function, it created a reduced order model approximating a flaw's stress intensity factor. The resulting model requires two essential components: function weights, and stress intensity factor influence coefficients (SIFICs).

The initial cost of using this method can be fairly significant, as it requires many different flaw analyses to be performed. However, after the results have been obtained, this reduced order model can be used to evaluate many different flaws very rapidly for many types of simulated events.

A required step in this approximation is the development of the global RPV finite element model. This is a model of the un-cracked RPV wall, which is used to measure the

RPV's thermomechanical response to the time dependent pressure and temperature boundary conditions. Using this model, the normal stresses in the RPV wall are obtained at various radial positions through the entire wall thickness. The stress distribution through the thickness of the RPV wall can then be found using the radial coordinates and corresponding normal stresses. The function weights are obtained by creating a polynomial that describes the stress as a function of radial position in the wall. For the analyses performed in this thesis, a third order cubic polynomial was found to be an adequate approximation [11], and was thus used to describe the normal stress in the RPV wall, as shown in Equation 2.1.1 below:

$$\sigma(a') = w_1 + w_2\left(\frac{a'}{a}\right) + w_3\left(\frac{a'}{a}\right)^2 + w_4\left(\frac{a'}{a}\right)^3 \tag{2.1.1}$$

where in the above equation $\sigma(a')$ is the normal stress in the RPV wall as a function of the radial distance *a'* spanning from zero to the length of the hypothetical flaw of interest, *a*. The coefficients, *w*, of the polynomial are used in the reduced order model's final approximation as the function weights, as shown below in Equation 2.1.2.

$$K_I = \sum_{i=1}^{n} w_i K_i^* \sqrt{\pi a} \tag{2.1.2}$$

Where K_I is the stress intensity factor, K_i^* is the stress intensity factor influence coefficient, and *a* is the flaw depth measured from the inner most open surface. The value for *n* is determined based upon the form of the polynomial used to describe the stress in the un-cracked RPV wall. Both the influence coefficients and function weights are indexed on *i*, which contains the integers from one to four, as it was previously determined that a cubic polynomial most accurately captured the stress distribution resulting in four coefficients.

As previously discussed, and shown in Equation 2.1.2, the reduced order model requires a second component, or rather set of components: the stress intensity factor influence coefficients or SIFICs. Eventually, Equation 2.1.2 will be evaluated by selecting the appropriate values from a library of existing SIFICs. However, it is important to first discuss the methodology for creating this database. Developing a library of SIFICs can be a long a costly process requiring the development and evaluation of several finite element crack models. Although the initial cost is high, the benefit is that once the database of influence coefficients has been created, no additional finite element crack models are required to use the reduced order model.

A primary function of the stress intensity factor influence coefficients is to use the effects of RPV and crack geometry in order to influence the final stress intensity factor solution. SIFIC models are parameterized such that the library of solutions is representative of a wide array of geometry characteristics, such as relative flaw depth, flaw aspect ratio, or any other geometric property of the RPV flaw model.

SIFIC models are created as a cracked portion of the RPV wall, which throughout this thesis will be referred to as an RPV sub-model. In each sub-model, the geometry of the flaw and RPV are pre-determined and physically represented. Recall that this method uses the principle of superposition, where specifically, the effects of the combined loading in the RPV wall are broken down into individual components corresponding to the coefficients describing Polynomial 2.1.1. The SIFICs are used to capture the effect of specific RPV and crack geometry characteristics when subject to each of the loading components captured by the stress polynomial. The loading effects specific to the PTS event are therefore represented in the stress coefficients, and thus the boundary conditions applied to the SIFIC models are

generalized in order to be valid for any loading scenario that can be described using a cubic polynomial. Thus, a series of unit pressure loads corresponding to each term in Equation 2.1.1 is individually applied directly to the face of the flaw, where a single sub-model is evaluated four different times in order to create the required four SIFICs. Thus, if the analysis is performed in this order, the number of sub-model evaluations required for the library of solutions is determined by the number of coefficients used to describe the stress polynomial.

Additionally, by the method of superposition, it was shown that the pressure loads can be applied directly to the surface of the flaw [12], as opposed to the more traditional method of applying the pressures at a far surface paralleling the flaw. This method is shown in greater detail in the figure below:

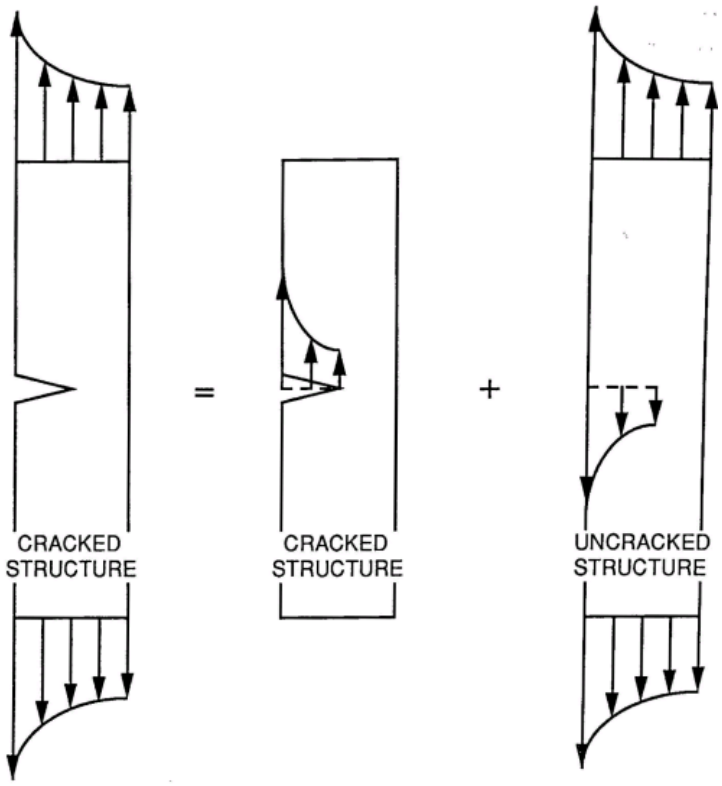

Figure 2.1.1: Cracked Structure Loading Using Superposition Principle [11]

Figure 2.1.1 illustrates the concept of superposition being applied to a crack model. The overall system is shown in the image on the left, where the cracked structure is loaded at both ends of the domain. The process of obtaining the SIFICs is found as a result of the loading shown in the middle picture, where the cracked structure is loaded by applying a pressure load directly to the face of the flaw. As mentioned previously, the pressure loads vary in order to correspond with the weights describing Polynomial 2.1.1. In this work, it was determined that a cubic polynomial containing four terms adequately described the stress in the crack-free RPV wall. Thus, four influence coefficients are required corresponding to the uniform, linear, quadratic and cubic terms. The loading scenarios applied are shown below in Figure 2.1.2, where each is applied separately in order to obtain four SIFICs.

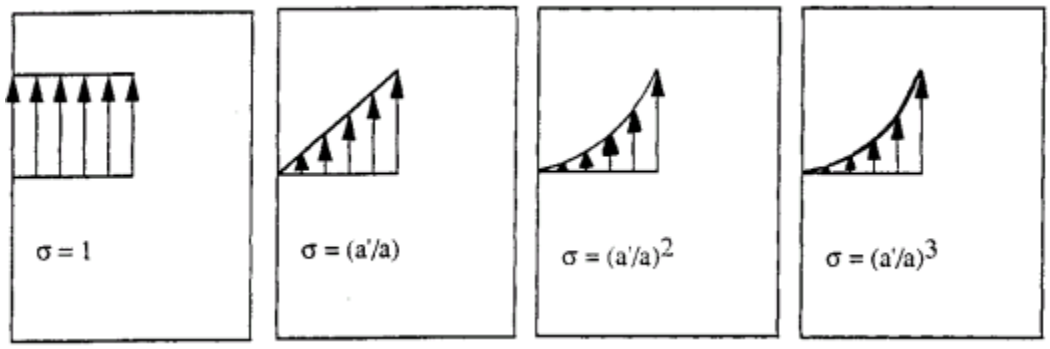

Figure 2.1.2: Crack Face Pressure Profile [11]

In Figure 2.1.2, the loading applied is a unit pressure load applied to the face of the flaw such that the distribution can be defined by a purely uniform, linear, quadratic or cubic function with a maximum magnitude of 1. Upon loading a single model, the flaw can be analyzed in order to obtain the corresponding stress intensity factors. From Equation 2.1.2, the influence coefficient is found by dividing the stress intensity factor by the square root of pi times the flaw depth. As shown in the equation below:

$$K_i^* = \frac{K_\mathrm{I}}{\sqrt{\pi a}} \tag{2.1.3}$$

Where K_i^* is the stress intensity factor influence coefficient corresponding to the loading applied, *a* is the flaw depth measured from the inner most surface to the tip of the flaw, and K_I is the stress intensity factor obtained from the pressure load applied to the face of the flaw.

The process described above can then be repeated multiple times in order to develop a library of these influence coefficient values, where the finite element model in parameterized such that many different flaw and RPV geometric properties are considered. In parameterizing the models, a database is created, from which values corresponding to the flaw geometry of interest can be accessed and used in Equation 2.1.2 for rapid stress intensity factor calculations.

Now that the function weights and SIFICs can be obtained, Equation 2.1.2 can be evaluated in order to approximate a final stress intensity factor. However, the method of selecting the appropriate set of SIFICs has yet to be fully addressed. Recall that the database of SIFICs is a library of discrete input values. Thus one obvious approach is to require those specific discrete inputs in order to make the approximation. However, the ability to use any continuous input would be more useful as it would enable the evaluation of more flaws. Fortunately, this can be accomplished in a number of ways through the use of surrogate models and will be discussed further in chapter 3.

It is worth noting that, in the solution path outlined above, the stress distribution was used to drive the entire process of developing this reduced order model. In this approach the majority of the emphasis was placed on accurately describing the stress in the RPV wall, resulting in a requirement of four SIFIC values. This seems to be the logical approach as the

designer is free to use any polynomial form for equation 2.1.1, allowing for an accurate representation of the RPV's thermomechanical response. However, if instead, a library of SIFICs was created without any prior knowledge of the stress distribution in the RPV wall the method can still be valid. Though one foreseeable issue with such an approach is that a limit is placed on the order of the polynomial that can be used to describe the through wall stress in the RPV. Therefore, even though it is not explicitly required to perform the global model evaluation as the first step in this process, the library of SIFICs should be created with some pre-existing knowledge of the stress distribution in the RPV wall for the simulated event of interest.

After evaluating the global RPV response and creating a library of SIFICs, the stress intensity factors for many different flaws can be determined in a fraction of a second using equation 2.1.2. This is very useful for probabilistic analyses, where in general millions of deterministic results are required. For this reason, the method described above is used extensively within the FAVOR code. Its developers have previously created a large database of SIFICs using the results from several Abaqus fracture models, as well as developing their own global RPV model within the code framework. More on the applications of FAVOR, as well as the theory utilized in the code will be discussed in the following section.

2.2 FAVOR

The FAVOR code is a simulation tool developed to perform risk informed analyses of embrittled RPVs when subjected to various types of transient events [11], and is capable of accommodating a large number of elliptical flaws including fully embedded, inner and outer surface breaking axis aligned flaws. It was originally derived from models developed in the early to mid 1980s in an effort led by the Nuclear Regulatory Commission (NRC) to re-

evaluate its PTS regulations. FAVOR was developed for the NRC by scientists in the Heavy Section Steel Technology program at Oak Ridge National Laboratory and is maintained as the base-line NRC selected applications tool for assessing PTS regulations to insure that RPVs maintain their structural integrity during off-normal operating conditions [11].

This code is a highly capable and versatile tool with a number of useful applications, many of which were beyond the scope of this project and thus were not utilized in this research. The primary focus of this research involves the method utilized by FAVOR in its deterministic analysis of axis aligned, surface breaking elliptical flaws. Specifically, the weight function method described in section 2.1. This is accomplished in FAVOR by utilizing a library of Stress Intensity Factor Influence Coefficients (SIFICs), previously developed by researchers at ORNL using Abaqus. The global RPV's thermomechanical response is found using a finite element solver developed within the FAVOR code framework. [11]

2.2.1 FAVOR - Framework

Probabilistic analyses are conducted within FAVOR through the use of Monte Carlo simulations, a method which was briefly described in Chapter 1. A Monte Carlo simulation will take far too long to reach a usable solution if the model used in the simulation takes hours or even minutes to produce a single result. This is due to the fact that useful results often require millions of model evaluations. One way to mitigate this issue is to create a reduced order model, which can be evaluated much faster as a surrogate for the more complex model. The developers of FAVOR have implemented surrogate modeling into FAVOR's probabilistic module by using the weight function method described in chapter 2.1. Where, instead of running a finite element model to determine the stress intensity factor

for each random flaw within the Monte Carlo simulation, the stress intensity factor is found using the weight function method which can be evaluated in a fraction of a second, and comes at a minimal reduction in accuracy.

FAVOR conducts its deterministic analysis using two modules. The first is FAVload, a module that uses built in finite element code in order to evaluate the crack free RPV's global thermomechanical response to some transient event. This is a deterministic model where time dependent boundary conditions can be applied to the RPV in order to simulate a PTS event. This module takes in the material properties and geometry for the RPV, as well as the boundary conditions for the thermal-hydraulic event and uses finite element analysis to output the material's temperature and stress as a function of position and time. Again, this analysis is limited to the crack free beltline region of the RPV wall and was therefore simplified to a 1D axisymmetric model.

The next step in FAVOR's analysis is conducted in FAVpfm, a module created to conduct probabilistic fracture mechanics analyses using Monte Carlo simulations. In order to perform probabilistic assessments, FAVpfm is required to evaluate the stress intensity factor using the deterministic weight function method described in section 2.1. As such, this module can also be used as a purely deterministic model, to find the stress intensity factor for a given flaw. The module is supplied with a continuous flaw depth value, which must be within the domain of the SIFIC library. Additionally, the FAVload output data file is required, which provides normal stresses found from the crack free global RPV model. This is required in order to determine the function weights describing Polynomial 2.1.1, which are then used in Equation 2.1.2.

One limitation in the analysis conducted within FAVOR is its method for the selection of the appropriate SIFICs for any given flaw. Particularly, the only parameter describing the flaw that can be varied as a continuous value to obtain a solution is the flaw depth relative to the wall thickness. This is accomplished by interpolating solution values, though the exact interpolation scheme is not specified. Therefore, for each deterministic analysis of a single flaw with a specified depth, a stress intensity factor is output for each of the different aspect ratios contained within FAVOR (2,6,10, infinite).

This result presents a limitation in FAVOR's analysis capability, where the ability to determine the stress intensity factor for any continuous aspect ratio would enable a better representation of the RPV's flaw distribution. For the analysis performed in FAVOR, this a very minor detail, and would not likely have a significant impact on the overall analysis results. However, in the interest of modeling off axis 3D flaws, being limited to discrete inputs could become problematic because the flaws will need to be described by additional input parameters.

2.2.2 FAVOR – Theory

A large portion of this research was focused on investigating the extension of the weight function method to off axis flaws. FAVOR has already implemented this approach in its analysis of axis aligned flaws, thus its methods and results were of significant importance to this study. Furthermore, FAVOR's wide acceptance by the NRC and the scientific community make it an excellent benchmark in the validation of models developed in this research. Much of this section will closely resemble that of section 2.1, as FAVOR utilizes the weighting function method for much of its analysis. Though in Section 2.1, the presence of cladding was not discussed. This detail adds some complexity to the analysis, and will be

addressed throughout this section.

For purely deterministic analyses of circumferential or axial inner surface breaking elliptical flaws in the presence of cladding, FAVOR determines the stress intensity factor for Mode I loading using the following equation:

$$K_I = K_{I_{\text{base}}} + K_{I_{clad}} \tag{2.2.1}$$

As shown above, the total stress intensity factor solution, K_I, is found by calculating the stress intensity factors for the base material and cladding individually. The respective K_I values are calculated using the principle of linear superposition discussed in section 2.1. For the base material, the application of this principle is identical to the process outlined in section 2.1. For the cladding, that process requires some modifications, which will soon be presented in great detail. Though the order in which these two components are obtained is completely insignificant, the process for determining $K_{I_{\text{base}}}$ will be described first.

The method for obtaining the stress intensity factor for the base material is a direct application of the method described in chapter section 2.1. Recall that the solution requires the evaluation of the global crack free RPV finite element model, from which the stresses and corresponding locations within the RPV wall are stored in a database. Additionally, a library of SIFICs is required, of which researchers at ORNL had previously developed using Abaqus. Using elements from each of these components, the following equation can be used to determine the stress intensity factor for the base metal, where, in this step, the cladding is completely ignored.

$$K_{I_{base}} = \sum_{j=0}^{3} C_j K_j \sqrt{\pi a} \tag{2.2.2}$$

In Equation 2.2.2 above, a, is the flaw depth, K_j are the SIFICs, and C_j are the

function weights, both of which are indexed on *j*. The function weights are obtained using a least squares polynomial fit [11], and correspond to *w* in equation 2.1.1, shown again in Equation 2.2.3 below:

$$\sigma(a') = C_0 + C_1\left(\frac{a'}{a}\right) + C_1\left(\frac{a'}{a}\right)^2 + C_1\left(\frac{a'}{a}\right)^3 \quad (2.2.3)$$

Where in [11] it was determined that a cubic polynomial adequately described the RPV wall stresses for this particular event. It is important to recall that this analysis is for a transient process, a PTS event. Therefore the global RPV model is subjected to boundary conditions that vary over time, and is evaluated at each time step specified in the sequence. This means, at each time step in the simulation, the stresses at each of the radial positions will change. Thus, the coefficients in equation 2.2.3 must be determined and stored for every time step in the simulation. Additionally, new coefficients must be determined for every flaw length that is considered in the deterministic analysis. This is shown by Equation 2.2.3, where *a'* is a radial distance spanning from zero to *a*, which is the depth of the flaw being evaluated in the deterministic analysis. Because the polynomial is fit over the length of the flaw being considered, the polynomial must be determined for each flaw that is analyzed. This process can be repeated for any flaw length, *a*, such that the value is contained within the domain of SIFIC data.

Upon calculating the stress intensity factor for the base metal, where cladding effects were not considered, the next step is to determine the stress intensity factor for the cladding, although it should be noted that the order in which these components are obtained is not important. The stress intensity factor for the cladding is determined through the application of the weighting function described in section 2.1 and shown in 2.2.4 below:

$$K_{\mathrm{I}_{\mathrm{clad}}} = \sum_{j=0}^{1} C_j K_{clad\,j} \sqrt{\pi a} \tag{2.2.4}$$

Although the above equation maintains the same form as equation 2.2.2, it illustrates two differences between the two equations. First, the indexing has changed. For the base material, a cubic polynomial was used to describe the stress distribution through the RPV wall, where for the cladding analysis, the polynomial shown in Equation 2.2.3 is truncated after the linear term, thus the reduction in the index. The second difference is the added subscript "clad" attached to the stress intensity factor influence coefficient term. This was added to show that the SIFICs for the base and cladding materials are separate values, and cannot be used interchangeably. This will be discussed in greater detail in section 2.2.3, when the specific geometric parameters for the SIFICs are introduced.

In addition to differences in the polynomial forms, the process utilized by FAVOR to obtain the cladding weights, C_j, is not the same process used to obtain the weights used in the base material. The cladding function weights require the coefficients from two separate linear stress polynomials, as opposed to just one for the base metal. The first, is a linear least squares fit of the stresses in the cladding as a function of the corresponding radial positions. This polynomial is fit over the full length of the cladding material and is not related to crack depth. The resulting polynomial is described by two coefficients, which will be referred to as the actual coefficients. The next set of coefficients are obtained by extrapolating a line through the thickness of the cladding using the two inner-most stress values located within the base material. The final coefficients used as the function weights in equation 2.2.4 are obtained by subtracting the extrapolated coefficients from the actual coefficients.

Once the coefficients for the cladding have been determined, the appropriate SIFICs

can be selected and used in Equation 2.2.4 in order to determine the stress intensity factor for the cladding. The final result can then be determined using equation 2.2.1, where the base metal and cladding stress intensity factors are summed, resulting in the total stress intensity factor for the flaw of interest.

2.2.3 FAVOR - Application

Up to this point, the stress intensity factor influence coefficients have been presented in a mostly general way as values which are used in the approximation method to represent crack geometry and its effect on the overall solution. In this section, the specific details of FAVOR's library of SIFICs will be presented. FAVOR's library of SIFIC data was used extensively throughout this research, particularly in the work documented in chapter 3.

Using the approach described in section 2.1, researchers at Oak Ridge National Lab (ORNL) developed FAVOR's library of SIFIC data [12] using a number of Abaqus finite element models. The models were created for a relatively wide range of flaw and RPV geometry characteristics, such that the values contained within the database would be applicable to most pressurized or boiling water reactors. FAVOR's SIFIC data is available in appendix B of the FAVOR Theory and Implementation Manual [11] and was used extensively for this work.

Within this library, the SIFIC values reported are applicable for both axial and circumferentially oriented flaws, as it was shown in [16] that there is very little difference between the SIFICs for axial and circumferential flaws with a relative depth of $(a/t) < .5$. Additionally, all of the values used in this analysis were reported for a specific RPV geometry, where the inner radius of the vessel is ten times the thickness of the RPV wall. This parameter was determined in the development process as it is representative of most

PWR pressure vessel geometry [11]. In reference to Figure 2.2.1, the varying parameters used to describe the flaw geometry in the base metal include: flaw aspect ratio, (L/a), flaw depth relative to wall thickness (a/t), and angle along the flaw front (φ). Additionally, for the cladding, a fourth parameter corresponding to the cladding thickness was also included.

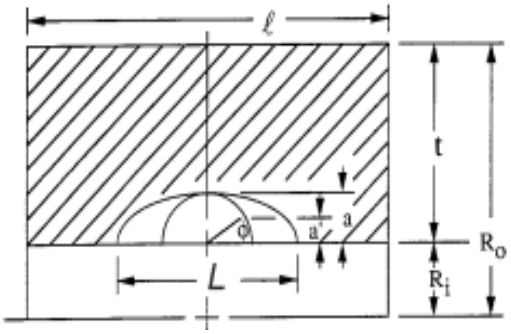

Figure 2.2.1: FAVOR's flaw geometry definitions [11]

Within FAVOR's SIFIC library, values are provided for the following finite set of crack aspect ratios: $(L/a) = [2, 6, 10, 999]$, flaw depths, *a*, relative to wall thickness, *t*, $(a/t) = [.01,\ .0184,\ .05,\ .075,\ .1,\ .2,\ .3,\ .5]$ and nine angular positions along the crack front $\varphi = [0 - 90]$, (non-constant increments). Additionally, for the analysis of the cladding, SIFICs are tabulated with respect to the additional parameter of the cladding's thickness using two finite values: .156 and .25 inches.

Currently, for surface breaking flaws, FAVOR is limited to aspect ratios of 2, 6, 10, and infinite, where these are discrete values fixed within the analysis. Also, even though the SIFICs are parameterized with respect to angular position along the crack front, FAVOR's results are limited to φ = 90. Therefore, the only crack parameter that can be varied as a continuous input value in FAVOR's deterministic analysis is the relative crack depth. This is accomplished in FAVOR using an interpolation scheme, the details of which are not made clear in their documentation.

While the methods utilized in FAVOR are efficient and adequate for 1D axis aligned flaws, the likelihood of an RPV containing only axis aligned flaws is very small. A large portion of this research was spent examining FAVOR's deterministic analysis in order to investigate the possibility of extending its methodology to off axis flaws. The addition of this capability would enable the probabilistic model to capture 3D flaws of arbitrary orientations, further increasing the effectiveness of the overall assessment. Upon conducting this review of the FAVOR code and its methods, it was determined that the current library of SIFICs would be inadequate for the goals of this project, as additional parameters describing the flaw orientation would need to be developed. Additionally, the ability to use any continuous value for a parameter describing the flaw would allow more flaws to be analyzed.

In pursuance of these goals, the INL's material aging, degradation and fracture mechanics code, Grizzly, will be used as the finite element analysis tool. Thus, the first step in the process is to verify that the methods used within FAVOR's analysis can be implemented successfully using Grizzly as the primary material analysis tool. The implementation of the Grizzly code and its comparison to FAVOR will be the subject of the following section.

2.3 Grizzly

Grizzly is an application currently being developed within the INL's Multi-physics Object Oriented Simulation Environment (MOOSE) finite element framework. Grizzly is capable of modeling the material embrittlement and degradation in addition to solid and fracture mechanics in three dimensional transient analyses. In order to eventually extend the capabilities of the RPV analysis to 3D, Grizzly can be used to simulate the global thermo-mechanical response of an RPV during any process with time dependent temperature and

pressure boundary conditions. This model uses the inputs specific to the materials and time dependent boundary conditions simulating the PTS event, and outputs the normal stresses and corresponding radial positions in the RPV wall at each integration point.

As mentioned previously, the goal of this research is to use Grizzly in order to eventually extend the 1D axis aligned flaw evaluations performed in FAVOR to 3D off axis flaws. As Grizzly is a relatively new code, the first step in this process is to, in essence, re-create FAVOR's method for evaluating flaws deterministically using Grizzly as the FEA tool so that the results can be validated. The detailed approach and results of this process will be the direct focus of the subsequent section. As soon as FAVOR's deterministic surrogate model can be recreated using results obtained in Grizzly, the process for extending the functionality to 3D off axis flaws can begin.

2.3.1 Grizzly - Global Model

The first step in FAVOR's analysis can be recreated using the INL's Grizzly code as opposed to FAVOR's FAVload module in order to measure the response of the RPV wall. Grizzly has already demonstrated its ability to predict the material response of an RPV wall when subject to transient boundary conditions [5], though it will be demonstrated further in this thesis. Therefore, a global finite element model representative of the RPV's un-cracked wall will be created, and then evaluated using Grizzly. The Grizzly code utilizes the finite element method to calculate radial displacements, and through strain displacements and linear-elastic stress-strain relationships, the resulting hoop and axial stresses in the un-cracked RPV wall are determined. Time dependent temperature and pressure boundary conditions are applied to the inner surface of the model and vary over the course of 250 time-steps, where each time-step represents one minute. The stresses calculated at each step

include the effects from both mechanical and thermal stresses.

This particular simulation was designed by superimposing transient boundary conditions on the inner surface of the RPV, representing a PTS event. The particular event used in this demonstration was developed for the Beaver Valley facility and is shown in FAVOR as transient sequence number 130 [5]. All of the material properties, as well as the temperature and pressure histories used in this analysis were supplied in the FAVload input file. This scenario was found in [5] to be one of the large contributors to the total risk of RPV failure, and thus was the main focus of this research. The pressure and temperature conditions applied to the inner surface of the RPV wall are demonstrative of an event in which there is an initial cooling and depressurization, interrupted by a rapid re-pressurization, shown below in figure 2.3.1.

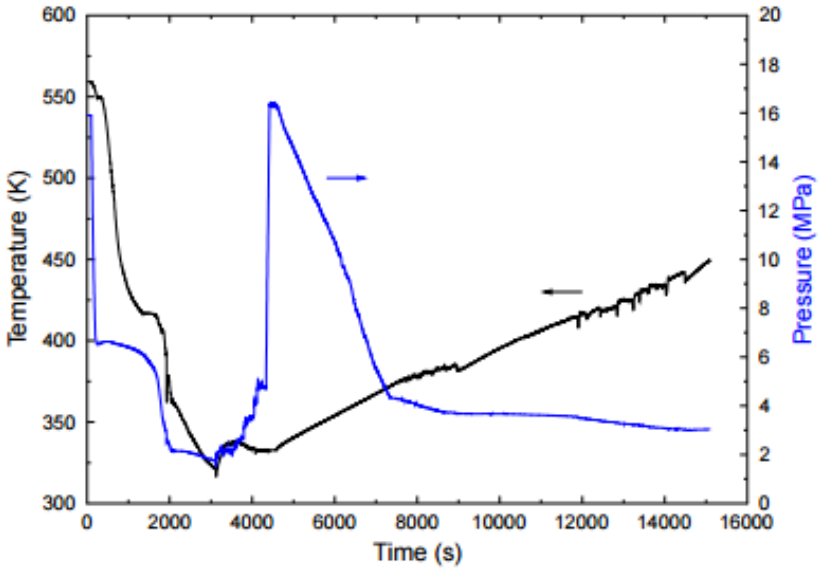

Figure 2.3.1: PTS Event 130 Pressure and Temperature Conditions [5]

The global model developed and used in this analysis is an un-cracked 2D strip of 45 quadratic surface elements with eight nodes per element, shown below. The inner surface of

the RPV is the surface on the left, and the mesh is biased at a ratio of 1.05 from the inner to outer surface. The innermost two elements are representative of the cladding, and the remaining elements are for the base metal. Each of the two materials was modeled using separate material properties, which were found in the FAVOR code. The bottom surface is fixed vertically, and the conditions shown in figure 2.3.1 are applied at the inner surface.

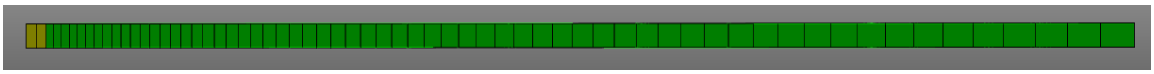

Figure 2.3.2: Global Finite Element Model Used in Grizzly Analysis

Additionally, constraint is then applied to the top surface that requires all nodes along the top surface remain in plane. This plane is then loaded using a scaled version of the pressure conditions shown in Figure 2.3.1, where magnitude of the scaling value is shown in Equation 2.3.1, given by [17]. The pressure is scaled and applied as such in order to account for the axial pressure, simulating a closed vessel.

$$P_s(t) = \left(\frac{R_i^2}{R_o^2 - R_i^2}\right) * P_i(t) \tag{2.3.1}$$

Where in the equation above, $P_s(t)$ is the scaled pressure as a function of time, which is applied to the top surface of the model. R_i and R_o are the inner and outer radii of the vessel, respectively, and $P_i(t)$ is the internal pressure with respect to time, which is shown in Figure 2.3.1.

As shown in Figure 2.3.2, the global model contains a very fine mesh near the inner surface of the RPV. This is not for mesh convergence, but efficiency in the overall evaluation. In order to perform a single deterministic analysis on one flaw, the global model is needed to output a series of radial coordinates and corresponding normal stress values, required to create polynomial 2.2.4. In order to fit that polynomial over the length of a flaw, there must be sufficient data, meaning at least four values, though more is desirable. The

most efficient way to do this is to create a global model with a tightly discretized mesh. If the mesh is very fine, especially near the inner surface, it can provide sufficient stress data to accommodate shallow and deep flaws. If the mesh is fine enough to supply sufficient data for fitting polynomial 2.2.4 over any of the flaws within the range of consideration, the global model is only required to be evaluated one time per transient.

For example, if the range of relative flaw depths being considered in the analysis is 10-30% of the total RPV wall thickness, the data limitation falls on the flaw at 10%. This is because the smallest flaw will have the lowest number of data points. Thus, if there is sufficient data to fit polynomial 2.2.4 to the smallest flaw in the dataset, there is sufficient data to fit the polynomial to any of the flaws within that range. This comes at a slight computational cost initially, as a very finely meshed global model will take more time to evaluate, which is insignificant for this analysis (minutes or even seconds). However, in the event that an actual 3D global RPV model was being analyzed, the additional computation time could be many hours. Regardless, the increase in efficiency is worth the added simulation time because the results for any flaw can be determined from one global model evaluation.

After the global model is evaluated, the resulting stresses and their respective coordinates are stored in databases containing the axial and hoop stresses and their corresponding radial positions. Recall that for the simulation of interest, there are 250 solution steps. Thus, at each step new boundary conditions are applied and the resulting stresses in the RPV wall will change. This means that the coefficients in equation 2.2.3 are required to be found at each step in the simulation. This can be accomplished by storing the resulting stresses and positions in a database, which can be accessed for each flaw analysis.

Furthermore, the set of coefficients required is only valid for the flaw being analyzed, as the polynomial is fit over the relative flaw depth, which can change for each flaw. Therefore, for each flaw, the coefficients at each time-step must be found, resulting in 250 sets of four coefficients, for one flaw (for the base metal). The same process applies for the cladding coefficients. After the necessary coefficients at each step have been determined, they can be used in equation 2.2.2 and 2.2.4 in order to obtain a final stress intensity solution for each time step.

In order to ensure that the Grizzly and FAVOR global models produce similar results, the following analysis was conducted. The conditions shown in figure 2.3.1 were used as temperature and pressure boundary conditions applied at the innermost RPV surface for each of the FAVOR and Grizzly global models. All material properties and RPV dimensions used in each of the analyses were identical. The scenario lasts 250 minutes and each minute is representative of one solution time-step. The following figures show the plotted solutions for the axial and hoop stress as well as temperature (respectively). All solutions were obtained at a point located 1 inch deep within the wall of the RPV (measured from inner-most surface). This point was selected at random, though other depths were also investigated and showed similar results.

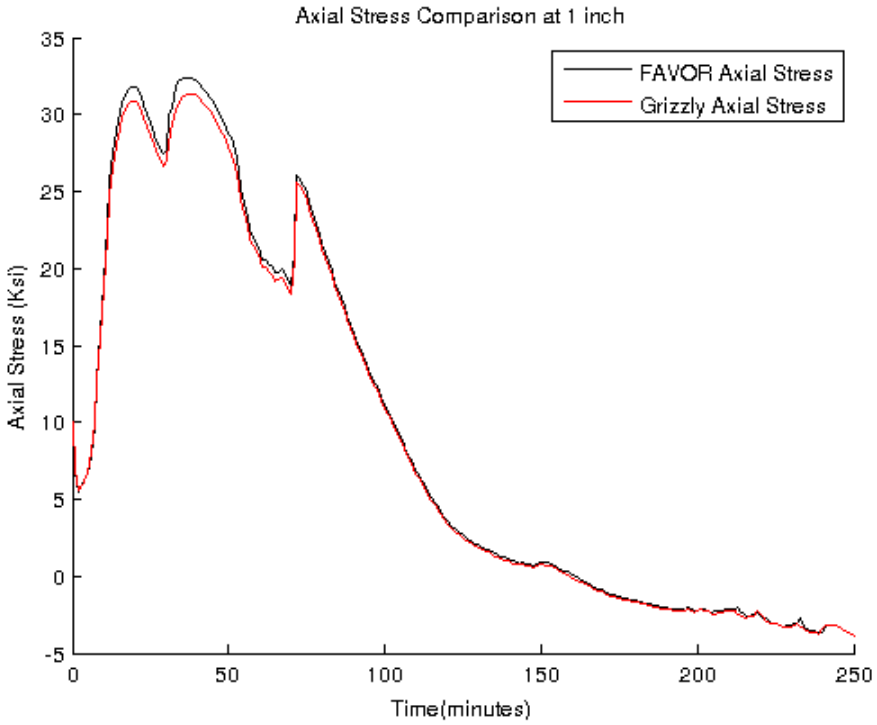

Figure 2.3.3: Global Model RPV Axial Stress Comparison

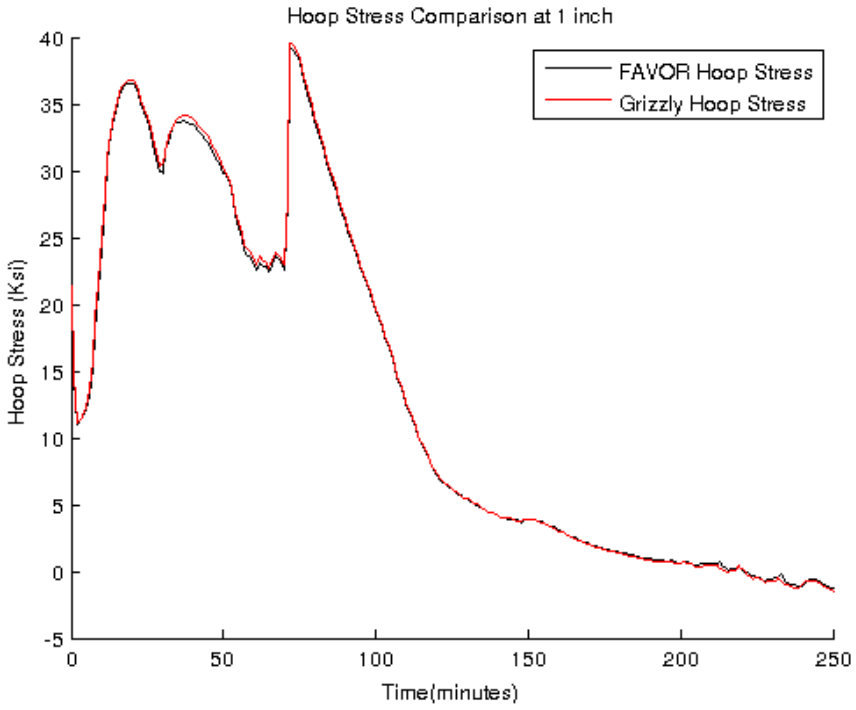

Figure 2.3.4: Global Model RPV Hoop Stress Comparison

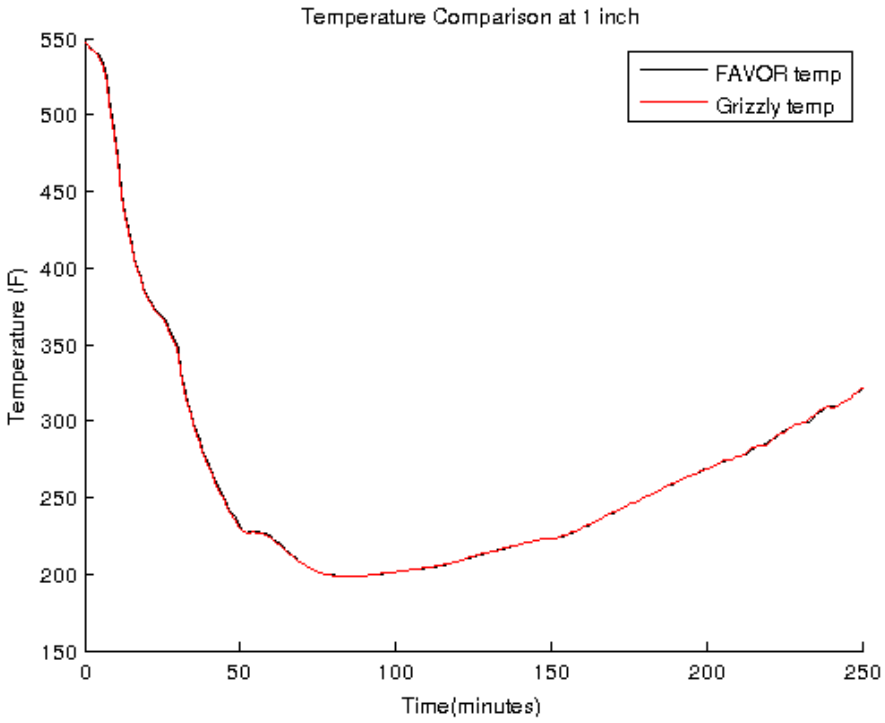

Figure 2.3.5: Global Model RPV Temperature Comparison

The resulting figures displayed above show good agreement between the Grizzly and FAVOR global models. This analysis was reasonably demonstrated in [5]. However, as the reduced order model requires polynomial coefficients obtained directly from the normal stress at points within the RPV wall, it was important to ensure that the global models mutually verify one another before proceeding to the next steps of the analysis.

2.3.2 Grizzly – Sub-models

It was mentioned previously in chapter 2 that the existing library of SIFICs used in FAVOR would be inadequate for the extension of the weight function method from 1D to 3D. Therefore, an expanded library of SIFICs, developed with respect to additional flaw parameters, will eventually be required and will be created using Grizzly. An appropriate first step in accomplishing this is to validate Grizzly's sub-model results using FAVOR's existing library of coefficient data. Once it has been verified that Grizzly can reproduce the same

library of influence coefficients utilized by FAVOR, new models, parameterized with respect to 3D flaw characteristics, can be developed. This capability could also be used to increase the accuracy of solutions within the existing range of data by increasing the amount of data within its current domain.

The specific process for determining the SIFICs is described in detail in section 2.1. In general, various unit normal pressure loads are applied directly to the face of the flaw such as to generate mode one opening. The pressure loads individually applied to the sub-model correspond to the terms in Polynomial 2.1.1, which for this case is a uniform, linear, quadratic and cubic term. The flaw sub-model is then evaluated four separate times to get four SIFICs (for the base metal). The four pressure loads can be described using the following equation:

$$P(x) = \left(\frac{x}{a}\right)^{i} \quad \text{where } i = 0,1,2,3 \tag{2.3.2}$$

In the above equation, *P(x)* is the pressure with respect *x*, the location along the face of the flaw, and *a* is the depth of the flaw in the model. Because the model is 3D, the load is then swept to encompass the entire face of the flaw being modeled.

In order to conduct these analyses, Linear Elastic Fracture Mechanics (LEFM) was used, which is valid under the assumption that the material in front of the crack tip behaves in a linear elastic manner. [8] The method utilized in Grizzly to evaluate the stress intensity factor of a given flaw is through the use of the J-integral. [18] For a flaw subject to pure mode one loading the stress intensity factor K_I can be found from *J* using the following relationships:

$$J = \begin{cases} \dfrac{(1-\nu^2)K_I^2}{E} & \text{for plane strain} \\ \dfrac{K_I^2}{E} & \text{for plane stress} \end{cases} \tag{2.3.3}$$

Where in the equation above, E is the elastic modulus, ν is the Poisson ratio, and K_I is the Stress intensity factor for mode one loading. [19] For the analyses performed in this research and common in RPV analyses [19], the plane strain relationship was used, as the vessel is closed at each end, and the wall is very thick. *J* is calculated within the Grizzly framework using the methodology detailed in [19]. Then, using the plane strain relationship shown in Equation 2.3.3, the stress intensity factor can be determined. The output K_I is then used in Equation to 2.1.3 in order to obtain the corresponding SIFIC.

As it was shown in study [16], there is little difference in the results of axial and circumferential flaws with depths spanning less than 50% of the RPV wall, thus SIFICs can be used interchangeably between the two orientations. For cracks beyond this depth, the orientation of the flaw has a larger effect on the stress intensity factor, and requires separate analyses for each orientation. Though, throughout this research, both axial and circumferential models were evaluated.

The model shown in the following figures was created in order to compare Grizzly SIFIC results with existing SIFICs supplied by FAVOR. This particular model is representative of a surface breaking circumferential flaw with an aspect ratio of two, which is defined in FAVOR as circular (see Figure 2.2.1). The flaw's relative depth is 10%, which for the RPV geometry being used is .865 inches (or .02197 mm).

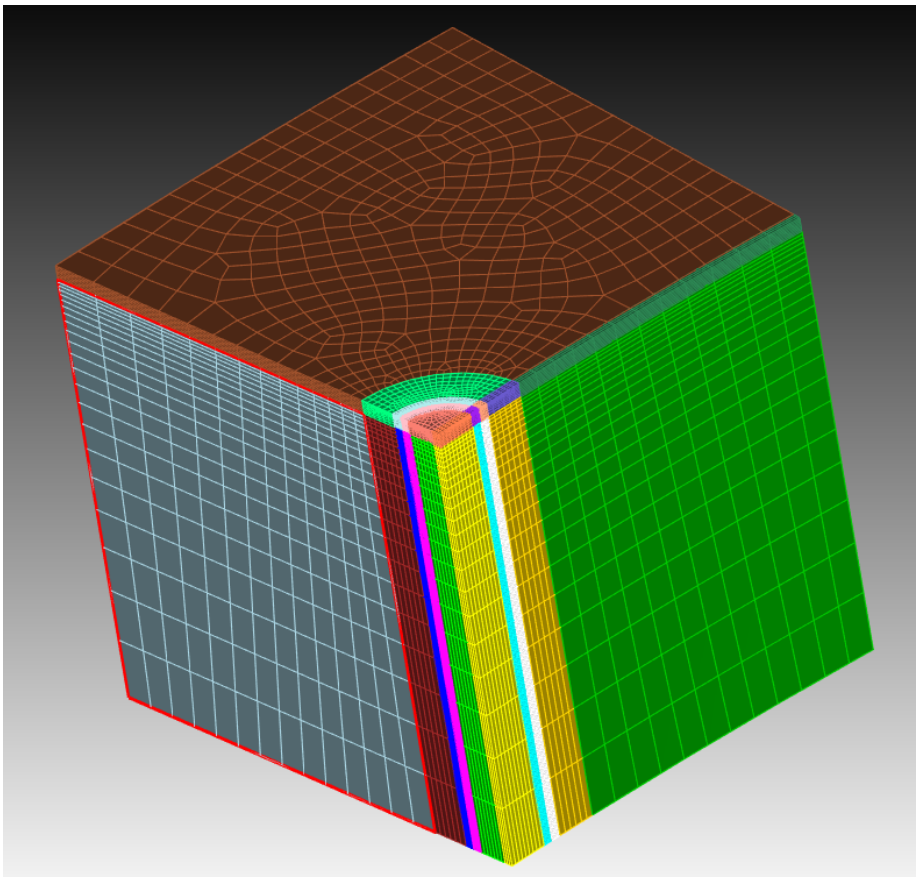

Figure 2.3.6: Circumferential Flaw Sub-model

The circumferential flaw model shown in figure 2.3.6 contains a thin layer of cladding, which can be seen as the thinner cut of material lining the front right face of the model. Additionally, in the above figure, there are a number of other cuts shown. It should be noted that, with the exception of the cladding, these cuts are not representative of different materials, they are simply zones within of the model which require a higher level of mesh refinement. For fracture models, a highly refined mesh is required in the vicinity of the flaw in order to obtain accurate solutions. The various cuts within the model were created to increase mesh refinement for specific zones in an effort to reduce model run time.

As made apparent by figure 2.3.6, the model's symmetry was utilized for efficiency. The sub-model shown above is representative of one quarter of a cracked RPV section. The

flaw is modeled as a sharp tip crack, and thus can be modeled as a completely flat meshed curve within the model.

The boundary conditions for this model were determined and implemented consistent with the process outlined in chapter 2.1. Recall that for the creation of the SIFICs, the sub-model is not subjected to the conditions seen by the RPV in a PTS event. Instead individual pressure loads are applied directly to the face of the crack in static single time-step analyses.

In Figure 2.3.6, the front right surface represents the curved inner surface of the RPV wall. For this analysis, both the inner and outer surfaces are free. The bottom surface is fixed in all directions in order to fix the model. The left surface is one of the symmetry planes used for efficiency. It intersects the flaw and thus requires symmetry conditions, where the displacements normal to that plane are specified as zero. Similarly, the model's top surface, excluding the face of the flaw, is also used as a symmetry plane, where displacements normal to the plane are specified as zero. In Figure 2.3.6 it is difficult to differentiate between the flaw front and the symmetry plane. The figure below provides a closer look of the top surface for the model shown in Figure 2.3.6.

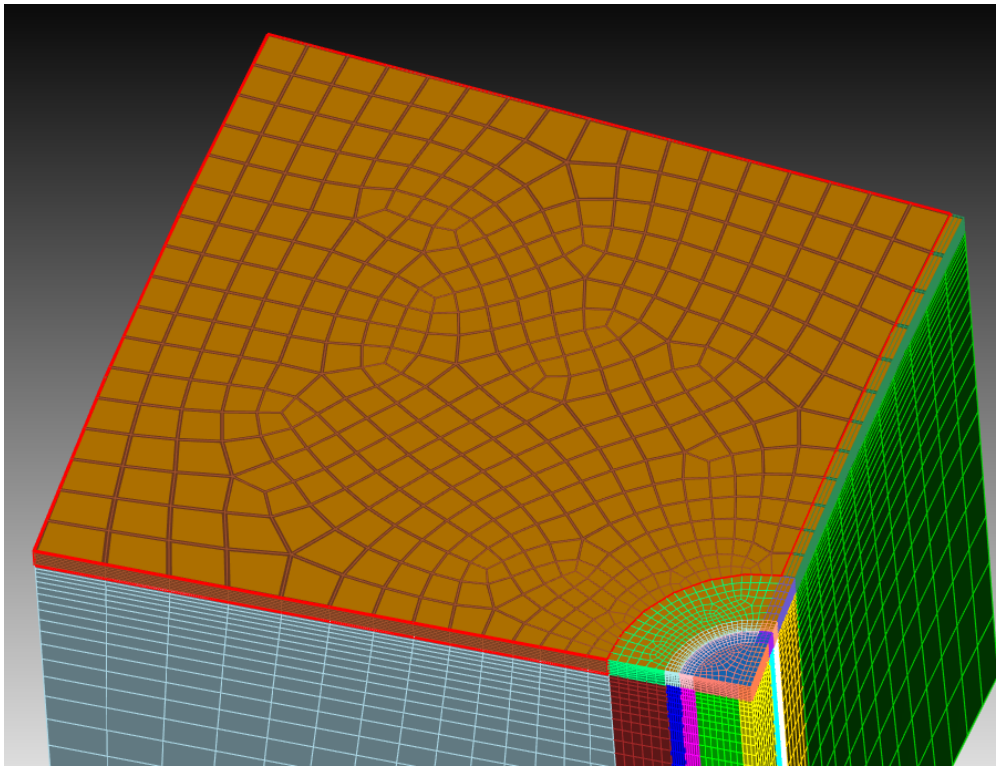

Figure 2.3.7: Top Surface Close Up of Circumferential Flaw Sub-model

The figure above shows a closer view the top surface of the circumferential flaw sub-model, where the surface highlighted in blue represents the flaw face. The portion of the top surface highlighted in orange represents the aforementioned symmetry plane, and is where the zero displacement boundary condition was applied (for displacements perpendicular to the plane).

As is the case with most finite element fracture mechanics problems, the meshing around the tip of the flaw is critical for a well-defined crack front as well as a fully converged solution. In order to accomplish this with computational efficiency, various cuts were made in the material in order to refine specific zones, particularly those closest to the front of the crack. The figure below shows the level of refinement required at the tip of the crack which was used for the evaluation of crack sub-models in this work.

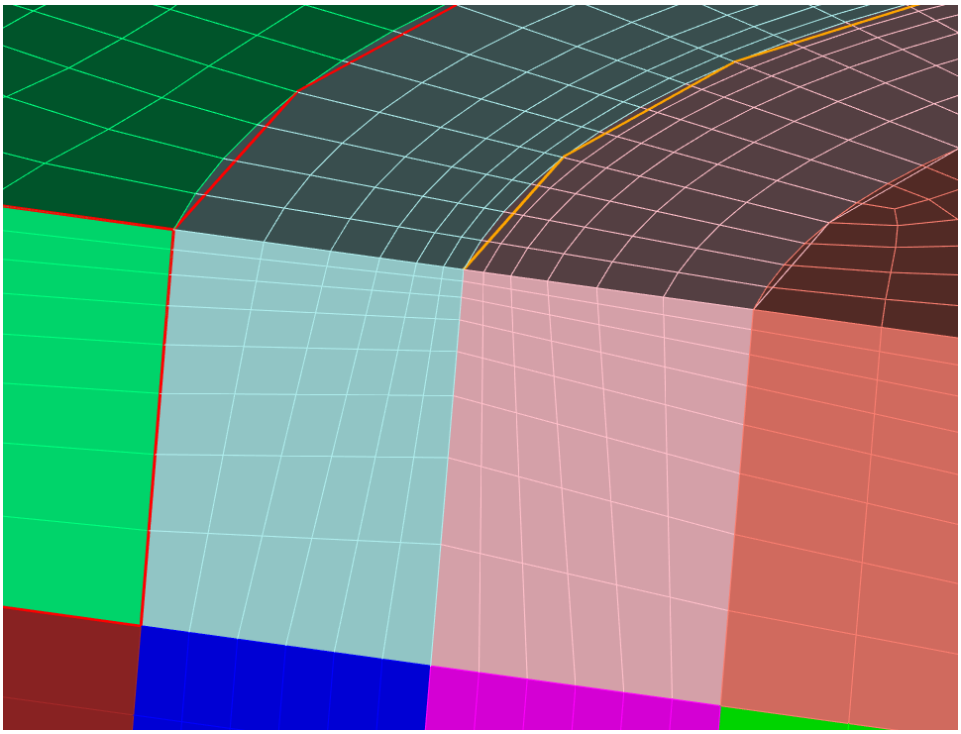

Figure 2.3.8: Crack Tip Level of Mesh Refinement

In the figure above, the flaw front is shown by the curve highlighted in orange. The mesh is biased towards the flaw at a ratio of 1.25. It should be noted that the curve on the flaw front appears to be unsmooth, as if it were comprised by connecting a series of small straight lines. This is not actually the case, just a limitation in the resolution of the graphical interface.

Using the model shown above, and the boundary conditions described above, the model was subjected to the four pressure loads previously introduced. For each load, the stress intensity factor was determined within Grizzly at each node along the 3D crack front. The SIFICs for the four terms were then found using equation 2.1.3. The resulting SIFICs were plotted as a function of the radial distance spanning from zero to the length of the flaw. The plots also contain the SIFIC values reported in FAVOR, which were determined using similar models evaluated using Abaqus. The results are shown in figure 2.3.9.

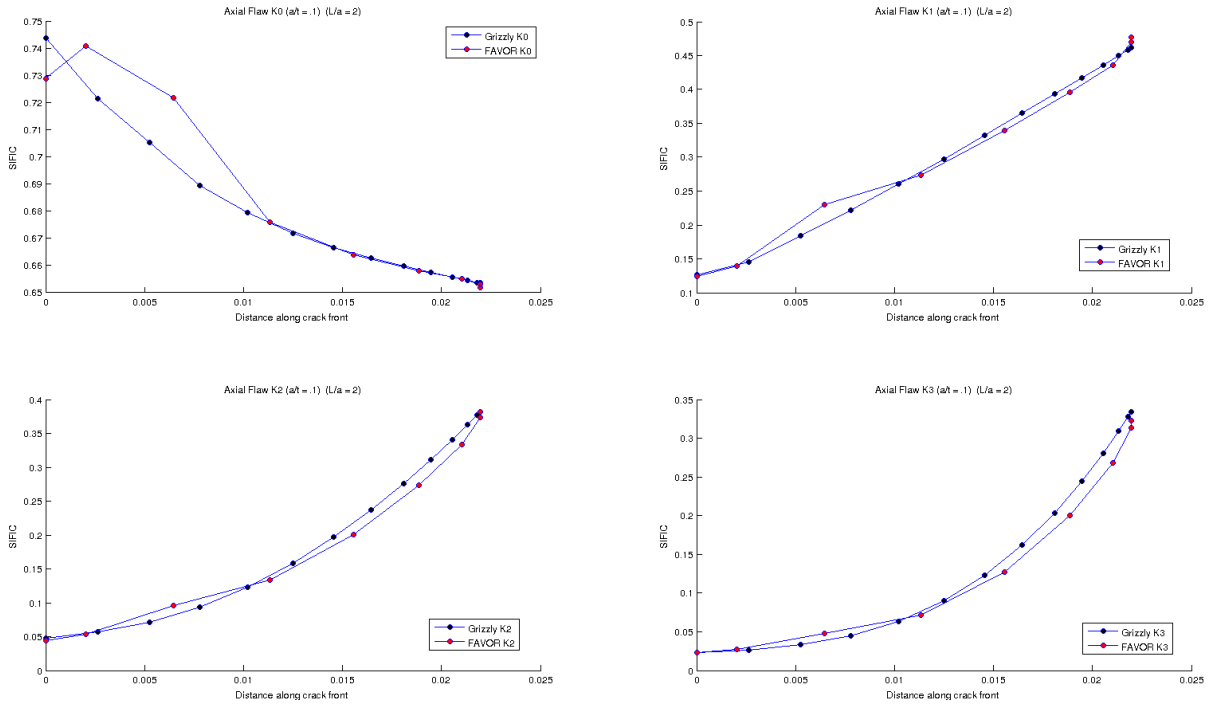

Figure 2.3.9: Grizzly/FAVOR SIFIC Comparison

The results above show relatively good agreement between the Grizzly and Abaqus solutions, although there is some disagreement which has yet to be explained. Therefore, at this point in the project, the SIFICs found using Grizzly have not been fully validated against the Abaqus solutions provided in the FAVOR documentation. There are a number of possibilities for this disagreement, many of which are currently being investigated by the Grizzly development team. This effort will be described in greater detail in Chapter 4 of this thesis.

Chapter 3. Surrogate Modeling

As previously discussed throughout in this manuscript, a large component in the solution method utilized in FAVOR is the selection of the appropriate SIFIC values. This is done in FAVOR by utilizing its large database of pre-existing influence coefficient values, where it interpolates between discrete flaw depths, but otherwise requires discrete flaw characteristics for inputs in its analysis. Additionally, the values supplied in FAVOR's SIFIC library are limited to the analysis of 1D axis aligned flaws. As the goal of this research is to eventually extend this analysis to 3D off axis flaws, the supplied library of coefficients is inadequate. Parameters that describe the flaw characteristics will need to include, at the very least, some representation of the flaw's orientation with respect to the RPV axes.

SIFIC data interpolation is a valid method for expanding the deterministic analysis to incorporate continuous parameter values. However, given the goals of this project, eventually the library of solutions will need to include much more data because additional input parameters will be required to fully describe flaws of any orientation. Interpolation schemes can range from simple to very complex but in general require a relatively tightly gridded dataset in order to capture the data adequately. [20] Additionally, capturing non-linear trends within the data can quickly add complexity to the scheme. These issues can be alleviated by creating a math model that represents the data, and is used as a surrogate for data selection.

There are many kinds of surrogate modeling techniques which can be utilized in order to represent the SIFIC data. The implementation of nearly any full interpolation scheme would be an improvement over FAVOR's method because the analysis would accommodate any continuous input, as opposed to only continuous flaw depths. This capability would

enable the analysis of a wider array of crack geometries, and would be better suited for future analyses in 3D.

Additionally, some math models could potentially capture trends within the data more effectively than interpolation. Surrogate models also have the potential to reduce complexity and the total data requirement in comparison with interpolation. When implemented, some models could potentially alleviate computational costs, increase fidelity and add functionality to the analysis. As such, the investigation of these modeling techniques could be very rewarding in relation to the goals of this project. Thus, in the following section, some of these data modeling approaches will be explored; their overall effectiveness will then be compared to determine their viability in the final analysis.

This demonstration will explore the utilization of three methodologies: linear interpolation, Least Squares Response Surface Methodology (LSRSM) and Gaussian Process Modeling, also known as Kriging. None of these approaches are limited to discrete inputs, therefore each method can be used to determine a continuous SIFIC given any continuous flaw characteristic input, so long as that input is contained within the domain of calibration data. Also, as it was previously shown that Grizzly SIFICs have not yet been validated, all of the models were calibrated using FAVOR's library of SIFIC data. Each of the methods will produce approximations of SIFICs when given input variables specified in section 2.2.3.

3.1 Interpolation

The first method considered for computing SIFIC values is multi-dimensional linear interpolation. Again, for surrogate model development, the SIFICs were not determined via Grizzly simulations, but instead using the pre-existing FAVOR database. As discussed in Section 2.2.3, the base material SIFICs are dependent upon three parameters: the flaw aspect ratio, relative flaw depth, and the angular position along the front of the flaw. Similarly, the

cladding SIFICs are output as a function of the same three parameters in addition to a fourth parameter: the cladding thickness, for which FAVOR provides two discrete values.

The interpolation scheme used in this step was selected for its simplicity, as well as for its similarity to the method utilized in FAVOR. However, FAVOR's Theory and Implementation Manual is not clear on the method of interpolation it uses in order to determine continuous flaw depths from discrete data values. Thus, the interpolation scheme used in this work was not developed to be a direct representation of the FAVOR solution, but rather a simple method that provides a close approximation. While interpolation is not likely to be the ideal method, it was chosen for demonstration purposes because it is a valid approximation technique.

For this analysis, Matlab's internal function "interpn" was used in order to perform n dimensional linear interpolation. The function "interpn" returns interpolated values for a function of "n" variables at a specific query point. Where for each of the material coefficients, the dimension of the interpolation corresponds to the number of input parameters (three for base metal, four for cladding).

This particular approach is of course limited in that continuous values falling between discrete points can only vary linearly. This insufficiency can be appeased by implementing higher order non-linear schemes or spline techniques, though these methods can be rather complex and more importantly, require more data. For this reason, interpolation schemes often require tightly gridded datasets in order to adequately capture the trends of the data in the undiscovered region of the design space. With future plans to implement this method in the analysis of off-axis flaws, significant computational effort would be required to gather sufficient data points for an accurate representation. While these drawbacks are not entirely

condemning, they must be taken into consideration when comparing surrogate modeling options for further implementation.

3.2 Least Squares Response Surface Methodology (LSRSM)

As stated previously, the method of selecting the appropriate SIFICs is limited in the FAVOR approach to strictly discrete values for aspect ratio and angle along the front of the flaw, and interpolation between relative flaw depths. Regression modeling can be used as an alternative method for determining SIFICs, particularly curve fitting. One such regression modeling approach, developed in 1951 by Box and Wilson [21], is Response Surface Methodology (RSM). This is a method of data curve fitting that requires the designer to determine the form of a polynomial expression of the input terms *a priori* [21], such that the model is linear with respect to the model parameters (i.e. polynomial coefficients). The polynomial of a specified form can then be created, where input and output data is used for calibration in order to determine the polynomial coefficients. The method for determining these parameters is dependent upon the size of the data used to calibrate the model as well as the number of terms specified in the model.

3.2.1 LSRSM - Theory

In order to demonstrate this method, consider the example of fitting a line to two points. Of course, in order to fit a line, two points are required. The line is then described with two parameters, as shown in Equation 3.2.1 below, where β_o and β_1 are the two model parameters corresponding to the y intercept and slope, respectively.

$$y = \beta_o + \beta_1(x) \tag{3.2.1}$$

When the number of model parameters matches the number of data points, the system is fully defined. This is shown in the following system of linear equations, where the number

of input data points, $n = 2$, and the number of model parameters, $\beta = 2 = n$.

$$\begin{bmatrix} y_1 \\ y_2 \end{bmatrix} = \begin{bmatrix} 1 & x_1 \\ 1 & x_2 \end{bmatrix} \begin{bmatrix} \beta_0 \\ \beta_1 \end{bmatrix} \tag{3.2.2}$$

Or, in short form:

$$\bar{y} = X\bar{\beta} \tag{3.2.3}$$

Where all y and x values are known coordinates corresponding to each of the two points. The model parameters can then be found by simply solving the system of linear equations, as shown in Eq. 3.2.4.

$$\bar{\beta} = X^{-1}\bar{y} \tag{3.2.4}$$

The coefficients needed to describe the line can be found by simply inverting the *X* matrix, and the resulting model (in this case, an equation for a line) will exactly predict each of the two points used in the calibration.

However, now consider the case where a model is being fit to three points instead of two. In order to predict the three points exactly, the designer could simply specify a quadratic form to the model. Likewise if there were 100 points, the designer could specify a polynomial form with 100 terms to accurately predict every calibration point. Intuitively, it would seem that this is the ideal approach, but in practice, it can easily result in an over-fit and often very noisy model. Furthermore, the emphasis of this modeling approach is not necessarily to predict known values so much as it is to predict unknown values. For instance, if the trend of a 10 point dataset is predominantly quadratic, the system should be modeled as quadratic, even though a 9^{th} order polynomial will capture every point, when the quadratic model will not. The higher order polynomial is simply capturing randomness or noise within the existing data, and as a result, will likely be less accurate in its predictions between known values. For these reasons, the form of the polynomial is specified *a priori*, where that form

can be chosen based upon some underlying physics, general simplicity or for any other reason determined by the designer.

For large datasets where there is more data than model parameters (i.e. $n > \beta$) the system is said to be over-defined, meaning the system contains more equations than unknowns, and a solution guaranteed to connect every point cannot be determined. When this is the case, the method of least squares can be utilized to find the best possible approximation. The least squares method is used to determine the model parameters, or calibrate the model, by minimizing the residual error between calibration data points and the model. Using this method, the model is unlikely to perfectly predict every calibration point, but can still adequately describe the trend of the data.

Recall from Equation 3.2.2, the example of a fully defined system of equations, where the number of calibration points (n) matched the number of model parameters (β). Let us instead consider the over-defined system, where the goal is to fit a linear model to a dataset with three input points. $(n = 3, \beta = 2)$ For this scenario, Equation 3.2.3 is modified to become Equation 3.2.5.

$$\begin{bmatrix} y_1 \\ y_2 \\ y_3 \end{bmatrix} = \begin{bmatrix} 1 & x_1 \\ 1 & x_2 \\ 1 & x_3 \end{bmatrix} \begin{bmatrix} \beta_0 \\ \beta_1 \end{bmatrix} + \begin{bmatrix} e_1 \\ e_2 \\ e_3 \end{bmatrix} \tag{3.2.5}$$

Where $\bar{e}$ is the model's residual error term, which is required to solve the system, as there are not enough model parameters to perfectly predict each calibration point. Additionally, one can see that X the matrix preceding the model parameters, is no longer square, and with the addition of $\bar{e}$, Equation 3.2.4 cannot be used to solve for the model parameters. Instead, the system is solved using the method of least squares. In order to apply this method, the over-defined system shown in Equation 3.2.5 must be expressed in short

form as Equation 3.2.6.

$$\bar{y} = X\bar{\beta} + \bar{e} \tag{3.2.6}$$

The method of least squares is used to calibrate the beta coefficients while minimizing the square of the error between the model and each calibration point, $\bar{e}$. Additionally, squaring the error term serves to penalize relatively large values. Thus, outlying points that are far away from the rest of the data have a smaller effect on the resulting model parameters. Therefore, using equation 3.2.6, the error term is solved for and both sides of the resulting equation are squared:

$$\bar{e}^2 = \left(\bar{y} - X\bar{\beta}\right)^2 \tag{3.2.7}$$

Recall that $\bar{e}$ is the error between the model's predicted value, and the actual data point. As such, the goal then becomes minimizing the square of the error. Therefore, the derivative of the squared error with respect to the model parameters, $\bar{\beta}$, is taken, shown in Equation 3.2.8.

$$\frac{d}{d\beta}\left(\bar{y} - X\bar{\beta}\right)^2 = 0 \tag{3.2.8}$$

Equation 3.2.8 can then be solved to find β after applying the derivative and performing some algebraic manipulation. The result is Equation 3.2.9, which can then be used to find the model parameters using the least squares method.

$$\bar{\beta} = (X^T X)^{-1} X^T \bar{y} \tag{3.2.9}$$

In the equation shown above, *X* is a matrix formed using the available data, then used to calibrate the model. The *X* matrix is populated such that it specifies the pre-determined form of the polynomial, accomplished by populating columns of *X* with data corresponding the desired polynomial terms. This is best demonstrated in an example. For instance, in fitting a quadratic polynomial, the matrix *X* is populated as such: the first column is

populated by a string of *n* ones, necessary to determine the intercept, β_0. The next column is populated with the un-altered input values for one variable, necessary for the linear term. The next column would be populated with those same data values squared, necessary for the quadratic term. Thus, the form of the polynomial is specified in the formation of the *X* matrix. The $\bar{y}$ term is vector of the outputs corresponding to each of the input data points in *X*. The result of the operation below forms $\bar{\beta}$ which is a vector of the coefficients corresponding to each of the terms in the specified polynomial, the size of which will correspond the ne number of columns in *X*. There is no limit on the number of inputs variables that can be represented using this method.

It is important to note that when utilizing this method, the scale of data values being considered is required to be approximately similar. As shown in Equation 3.2.9, the solution requires the inverse of $(X^T X)$ which is very difficult to compute accurately if the range of data within *X* is very large. The error is a result of the numerical methods used to perform the inverse, and can be remedied by properly scaling each of the variables before calibrating the model.

Scaling issues are especially the case when creating higher order non-linear polynomials. For instance, consider two independent variables, which are being used to fit a cubic response surface using equation 3.2.9. The first variable contains data ranging from .1-1, while the second contains values from 100-200. For a cubic response, the *X* matrix requires all of the data points to be cubed. As a result, the matrix to be inverted will contain values spread within the range of 1e-3 and 8e6. This is not a manageable spread of data, and thus the inverse operation would likely contain significant error. This however, can be easily fixed by dividing every value of the second variable by 200 before populating *X*. The result

will be a much more feasible range of 1e-3 to 1.

If the dataset is required to be scaled, it is imperative that when evaluating new points in the resulting model, the new inputs are scaled in a consistent manner. Additionally, there is no need to scale the vector of data outputs, $\bar{y}$, because they are not involved in any matrix inversions.

3.2.2 LSRSM - Implementation

In this work, the least squares response surface method was implemented twice to explore two different polynomial forms for the SIFIC as a function of the various flaw parameters. The first, Equation 3.2.10, is represented using cubic polynomial form. The second, Equation 3.2.11, is a quadratic model with first-order interaction terms, both of which are shown below:

$$K_j = \beta_0 + \sum_{i=1}^{n} \beta_i x_i + \sum_{i=1}^{n} \beta_i x_i^2 + \sum_{i=1}^{n} \beta_i x_i^3 \tag{3.2.10}$$

$$K_j = \beta_0 + \sum_{i=1}^{n} \beta_i x_i + \sum_{i=1}^{n} \beta_i x_i^2 + \sum_{i<j}^{n} \sum^{n} \beta_{ij}\, x_i x_j \tag{3.2.11}$$

In both Equations 3.2.10 and 3.2.11, β is used to represent the coefficients of the model to be determined, x_i represents each of the design variables corresponding to flaw geometry characteristics, and n is the number of characteristics being considered.

It is important to note that for this demonstration, the polynomial forms used were not chosen because they are the "best" (mathematically), nor is there any underlying physical phenomena shaping these functions. Instead, these forms were selected for their general simplicity for demonstration and proof of concept purposes. A rigorous approach would be to withhold a random subset of the calibration data to use instead as validation data, because these values have known outputs. Then, formulate a model and evaluate the model at the

validation points to determine the difference between the model and the actual outputs. Then repeat the process a large number of times for various model forms in order to determine the model form that produces consistently low error. While the basics of this strategy were used to determine the two forms used, there are likely more accurate forms, which were not considered.

As discussed in Chapter 2, complete flaw analysis requires six SIFIC values: four in the base metal and two in the cladding. Therefore, using FAVOR's SIFIC data, the two response surface forms were used for each of the six SIFICs - resulting in 12 equations corresponding to the forms shown in Equations 3.2.10 and 3.2.11. Where in both equations, *n* refers to the number of input parameters being modeled, which for the base material, $n = 3, x_i = \left[\varphi \ \left(\frac{L}{a}\right) \ \left(\frac{a}{t}\right)\right]$ and for the cladding $n = 4, x_i = \left[\varphi \ \left(\frac{L}{a}\right) \ \left(\frac{a}{t}\right) \ t_{clad}\right]$.

It is important to recognize that even though two responses may have the same form, the resulting model outputs can still be dramatically different. This is because, as illustrated in Equation 3.2.9, the coefficients are found as a function of the output data, $\overline{y}$, which is, in this case, the known SIFIC values which are different due to the loading conditions applied.

For reasons stated in section 3.2.1, the flaw characteristic data used in the population of *X* was scaled by dividing each vector of design variables (flaw characteristics) by its maximum value within the database. Thus, the scaling factors for the four design variables were $x_s = \left[\varphi = 90, \left(\frac{L}{a}\right) = 10, \left(\frac{a}{t}\right) = .3, t_{clad} = .25\right]$. This scaling operation thus resulted in a dataset where all normalized values fall between zero and 1.

While creating each of the response surfaces, the square matrix formed in the operation ($X^T X$) was found to be poorly conditioned, and could not be inverted accurately using Matlab. The matrix was poorly conditioned due to the appearance of linear dependence

naturally occurring within the data contained in X. This was a result of the fact that many of the flaw characteristics used as inputs are very similar to each other, because the discrete characteristics are repeated a number of times. For instance the supplied aspect ratios can be 2,6, or 10, the dataset for the base material contained 189 unique inputs, meaning 63 of the inputs all have an aspect ratio of 2. Likewise, there are only 7 discrete values for the relative flaw depth, so of those 63 inputs, 27 have an aspect ratio of 2 and relative depth of .1. The very closely related inputs become problematic, and thus induce numerical error when inverting large matrixes.

In order to reconcile this issue, the dataset was partitioned to avoid issues with numerical noise and improve the accuracy of the meta-model. The data was partitioned such that the calibration points used in the model formulation were closer to the point of interest. The partition primarily separated the larger flaw data from the smaller flaws. This was done without enforcing any continuity conditions at the boundaries for each of the partitioned datasets.

This issue exposes a limitation in the use of least squares response surface methodology for this application. Partitioning the data in such a way is certainly not the most computationally efficient solution to the problem, as it requires additional models to be created for each of the partitions, as opposed to one model for the full dataset. There are likely other, more efficient methods that would include filtering some of the data as well. Regardless, this issue, while not un-manageable, is something that must be considered when comparing surrogate modeling techniques for the selection in the final analysis framework.

3.3 Gaussian Process Modeling - Kriging

Another alternative to the SIFIC approximation methods utilized in FAVOR is

Gaussian Process Modeling, otherwise known as Kriging. This technique was originally developed in the field of geostatistics as a form of spatial variability modeling [22], where predictions of values a random field can be made with a quantified level of uncertainty. Though created for geostatistical applications, kriging is in essence, another form of interpolation or curve fitting, where the values that fall between calibration points are modeled as a Gaussian distribution governed by covariances as opposed to some sort of spline (interpolation) or error minimization (LSRSM) technique [23]. Unlike least squares RSM, ordinary kriging does not result in a closed form equation or a single deterministic value, but instead a function that produces a probabilistic representation of the output of interest, which is, in this case, the SIFIC.

With regard to the larger scope of this project, the surrogate modeling methods utilized will provide only an approximation of the SIFIC to then be used in some sort of probabilistic analysis. Again, the reason for performing a probabilistic analysis is to alleviate some of the uncertainties inherent within the system. Therefore, a data driven stochastic representation that accounts for the error in its prediction has the potential to be far more useful than a single deterministic output with no measure of the approximation's uncertainty. As such, Kriging was investigated as a potential means for surrogate modeling in order to represent SIFICs as a function of flaw characteristics. An overview of Kriging theory and its implementation will be provided in the following two sections.

3.3.1 Kriging - Theory

In Kriging, the output of interest is found based upon covariances associated with the spatial proximity of the point of interest and the rest of the data [24]. Consider a field of data points, where for each point, two or more known parameters describe a known output value.

The goal is to determine the output at a new point residing somewhere within the space of known points. In general, for interpolation schemes, the desired output is found using a weighted sum, where the weight values are created based upon their proximity to the point of interest. In Kriging, the weights are assigned according to a data-driven function. In this thesis, the particular kriging approach utilized is Ordinary Kriging.

In order to develop a kriging model, the spatial correlation of different points in the must be approximated throughout the design space. This approximation is made by using the existing data sampled throughout the space, measured through the use of a function called a semivariogram. The semivariogram expresses the spatial dependence between neighboring observations [25], specifically, a measure of the difference in covariance between any two points, where the covariance is a measure of how much two random variables change together. Meaning, if the semivariance between two points is zero, the points are perfectly correlated, and if the semivariance is large, the points are weakly correlated.

The first step in developing a semivariogram is to determine the lag, **h**, which is the distance between each possible combination of two points. The result of this operation is a very large dataset, as the distance between every combination of two data points has to be considered. For example, if 100 data points existed in the design space, where each point had two inputs, the result would be 4950 lag values contained within **h**. [26] The semivariance for each pair of points is then found using the following equation:

$$\gamma(\mathbf{h}) = \frac{1}{2 * num(\mathbf{h})} \sum_{i=1}^{num(\mathbf{h})} [y(\mathbf{u}_i + \mathbf{h}) - y(\mathbf{u}_i)]^2 \qquad (3.3.1)$$

Where in Equation 3.2.3, $\gamma(\mathbf{h})$ is the semivariance with respect to the lag, **h**. $\mathbf{u}_i$ is the location vector of point *i*, where *i* spans all integers from one to the number of total lag

distances, *num*(**h**). The output of a single point in the space is shown by $y(\mathbf{u}_i)$, and the output of every other point corresponding to each lag is shown by $y(\mathbf{u}_i + \mathbf{h})$.

The result of Equation 3.3.1 is typically a very large array of semivariance values, as it is evaluated for each lag. However, in the kriging process, a closed form continuous function representing the semivariance as a function of lag is required so that it can be evaluated for new points being estimated. The data output from the evaluation of Equation 3.3.1 represents the spatial correlation between each of the existing points. The ultimate goal is to use this data such that the spatial correlation can be measured between some new point of interest and the existing points. In order to do this, the semivariance of the field of data must be represented in a continuous function.

In order to determine a closed form representation of the semivariance with respect to lag, a curve can be fit to the semivariance data such that the data is described in closed form as a function of lag. This closed form representation is called the semivariogram, and is a critical component in the kriging model. In the final evaluation of the kriging model, the estimate of the sample point will rely heavily on this function. Additionally it should be noted that the semivariogram is only required to be determined once because it is formulated using the entire dataset and can thus be used for the prediction of many points.

In order for the kriging model to make a prediction, another parameter is required in addition to the semivariogram. This parameter essentially specifies a smaller range of data points closest to the point of interest, which can then have largest influence on the final estimate. This essentially localizes the effects of the model to the range of values closest to the point of interest. If for instance the number specified is six, the six points closest to the point of interest will have the largest effect on the final estimate. The lags are determined

between the point of interest and the six most immediately neighboring points, and are subsequently evaluated in the semivariogram. If the point of interest falls in a densely populated area of the space, the lags will be relatively short. Alternatively, if the point of interest falls in a sparse area of the space, the corresponding lags may be relatively large. Therefore, the semivariogram must be able to accurately determine the semivariance for wide range of lags.

Determining the appropriate semivariogram form can quickly become problematic because the dataset is likely very large and, as a result, very noisy. It is very difficult to accurately capture the trend of a dataset that is extremely large and noisy. However, there are a number of ways to alleviate these issues, one of which is to sort the data into bins such that all of the data is equally spread throughout each of the bins. The lag and semivariance are then averaged for each bin, and the dataset can be reduced to whatever size the designer chooses by setting the number of bins. This process of averaging effectively reduces the large scatter of data to a more manageable size, and can also reduce the effects of noise enabling the designer to select the best fit possible.

After sorting the data into bins, the semivariogram function can be approximated using any closed form expression selected by the designer. In general, the function describing the semivariogram will have two components which play a key role in further development of the model. These parameters are often called the sill and range, and are typically found at the point in which the semivariance begins to level off. Recall that the semivariance is a measure of the correlation between two points as a function of their distance, or rather their lack of correlation. As the distance between two points increases, their correlation should, in theory, eventually stop decreasing. The idea being that, at some distance, the points become

completely uncorrelated and thus cannot be any more uncorrelated, even though they may be spaced further apart. The value of the semivariance at which this happens is commonly called the sill and the corresponding lag is called the range. These values are used to describe the semivariogram function, and are thus obtained during the curve fitting process.

As mentioned previously, the kriging model requires a parameter which specifies the number of neighboring points to consider when predicting the output of some point of interest. The lags between the point of interest and each of the neighboring points are all determined and evaluated within the semivariogram in order to predict a final value. Although not required, the value corresponding to the range generally plays a large part in determining this number.

After the semivariogram has been formed, and the number of neighbor points to consider in the model has been specified, the final step is to determine the kriging weights, λ_I, as shown the equation below:

$$Y^*(\mathbf{u}) = m + \sum_{i=1}^{num(u)} \lambda_i [Y(\mathbf{u}_i) - m] \tag{3.3.2}$$

Where in Equation 3.3.2 shown above, $Y^*(\mathbf{u})$ is the estimated distribution of the output for the point of interest, **u**, *m* is a constant value which represent the overall mean of the existing data. An important assumption is that the estimate of the prediction is unbiased, such that the difference between the estimator's expected value and the true value is zero. The kriging weights, λ, can be determined such that the variance of the estimation's error is minimized. This expression is shown below:

$$\mathbf{K}\lambda = \mathbf{k} \tag{3.3.3}$$

Where the kriging weights relate the covariance between every possible pair of

neighbor points (**K**) to the covariance between the point of interest and each neighboring point (**k**) using the semivariogram. Both **K** and **k** are created using the semivariogram, existing data, and the point of interest. **K** is a matrix of all possible point-to-point covariances for each of the specified neighbor points. Consider an example where the number of neighbor points was specified as six. The first step is to determine the six data points that are closest to the point of interest. These points will be the neighbors used in the kriging model's prediction. The lags between every two point combination of the six neighbors are determined and evaluated in the semivariogram. The result is a 6x6 matrix of covariances between each of the neighbor points thus forming **K**. Next, the lags between the point of interest and each of the neighboring points is determined and evaluated within the semivariogram. The resulting covariances between the point of interest and the neighboring points are then arranged in **k**. Now that both **K** and **k** are known, the kriging weights can be determined.

Technically, the process outlined in the previous paragraph is for the method of Simple Kriging. In Ordinary Kriging, instead of assuming a constant mean, *m*, over the entire set of data the mean is assumed constant only over the set neighbor points being considered. This is valid only if the kriging weights sum to one. In order to minimize the error variance while satisfying this constraint, a Lagrange parameter is included, which forces the constraint to be obeyed.

The resulting expression is shown again by Equation 3.3.3, however there is an added term in the array of kriging weights, the Lagrange parameter. Thus, **K** must be augmented with an additional row and column of ones, with a zero for the bottom right diagonal term, where **k** has a value of one added for its final component.

After determining the kriging weights using the process outlined above, the estimated distribution of the output can be determined using Equation 3.3.4.

$$Y^*(\mathbf{u}) = \sum_{i=1}^{num(u)} \lambda_i Y(\mathbf{u}_i) \tag{3.3.4}$$

Where in Equation 3.3.4, $\mathbf{u}$ and $\mathbf{u}_i$ are location vectors spanning from the point being estimated (i.e. the input of interest) and the neighboring points being considered, indexed on *i*, for the number of neighbors, *num(u).* As mentioned previously, the number of neighboring points considered in the approximation of the output is determined by the designer. $Y^*(\mathbf{u})$ is the estimated mean of the distribution of the output.

Additionally, the following equation can be used in order to determine the variance associated with the estimated distribution.

$$\sigma^2 = C(0) - \sum_{i=1}^{num(u)} \lambda_i C(\mathbf{u_i} - \mathbf{u}) \tag{3.3.5}$$

Where in the above equation, *C(x)* is the semivariogram function, which when evaluated at zero is the value of the sill. This method stands out due to its ability to represent the level of uncertainty that exists in the model's prediction of values not provided in the data. Additionally, although kriging may seem complex, once implemented, it is very simple to use and does not require a lot of data to produce good approximations. In fact, it was shown in [27] that, when compared to splining in the prediction of real data, kriging outperformed splines by, at times, a considerable margin and never performed worse than splining.

3.3.2 Kriging - Implementation

It was stated in the previous section that the output from a kriging model is actually a

normal distribution of the expected output, as opposed to a single deterministic value. For reasons previously discussed, this quality has the potential to be quite valuable in future analyses. However, at this preliminary point in the project, the goal is to compare the various types of surrogate models, namely their outputs in an application that can be compared to the FAVOR solution. Therefore, for each SIFIC distribution output from a kriging model, only the mean value was considered and each was treated as a purely deterministic value. Future studies will utilize the full probabilistic representation in order to further refine reliability predictions.

As was the case for response surface methodology, a kriging model will need to be formed for each of the SIFICs needed for the analysis of a flaw. The result is six kriging models, four for the base metal SIFICs, and two for the clad. For each of the six cases, a semivariogram was constructed using the SIFIC data provided. The semivariogram describes the degree of spatial dependence in a random field of data. It can take on many forms, but for this demonstration only the following three curve forms were considered: Gaussian, exponential, and power [28]. The forms of each are shown respectively in equations 3.3.6-8.

$$f(x) = c * \left(1 - e^{\left(-\frac{3x^2}{a^2}\right)}\right) \tag{3.3.6}$$

$$f(x) = c * \left(1 - e^{\left(-\frac{3x}{\mathrm{a}}\right)}\right) \tag{3.3.7}$$

$$f(x) = cx^{\omega} \qquad where: 0 < \omega < 2 \tag{3.3.8}$$

Each of the three curve types were then fit to each of the six the semivariograms using a least-squares methodology. The data within the semivariograms was assembled into bins consistent with the process outlined in section 3.3.1. The number of bins used in each semivariogram was determined independently amongst the six models such that the curve

forms listed above would best fit the data. Upon fitting each of the three curve types to each semivariogram, the R-squared error was evaluated. The form with the lowest R-squared value for each individual curve was selected. In this study, it was found that all six of the semivariograms were fit most accurately using the Gaussian curve, shown in Equation 3.3.6. The resulting semivariograms are shown in the figures below:

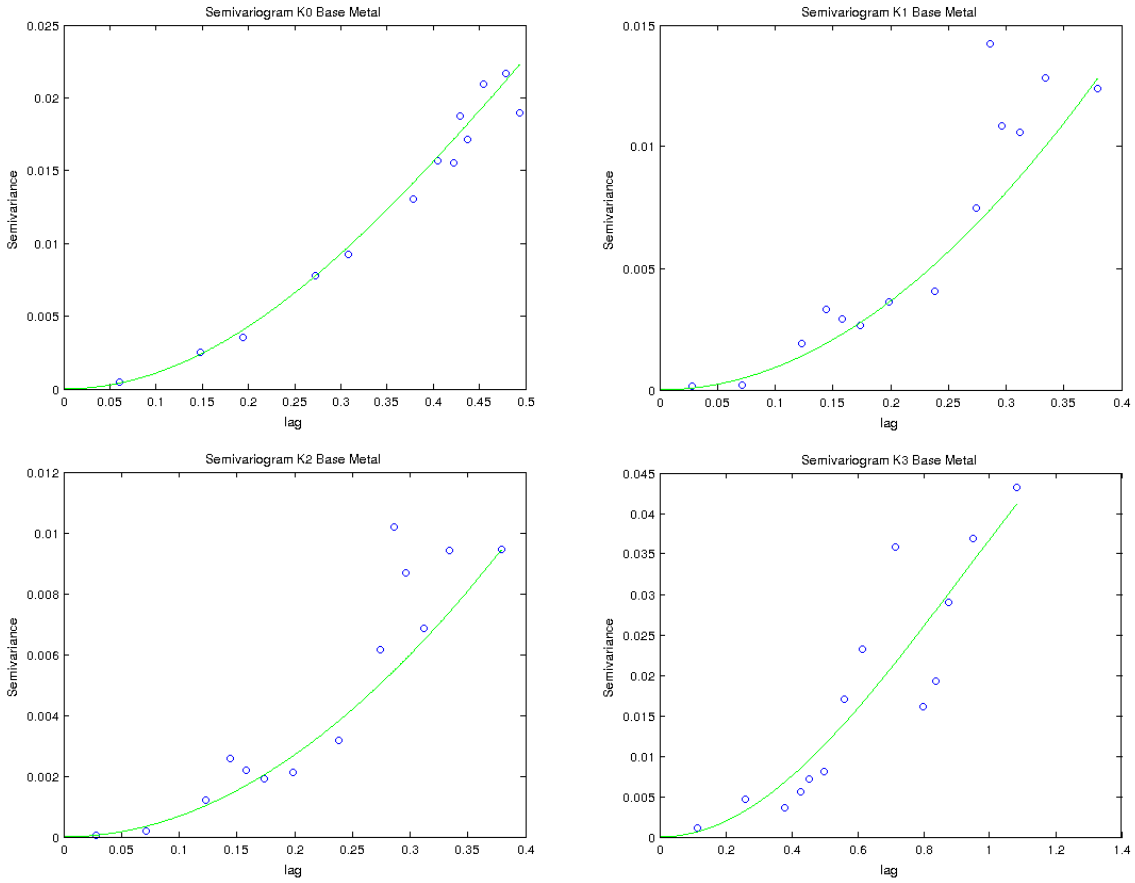

Figure 3.3.1: Semivariograms for Each of the Base Metal SIFICs

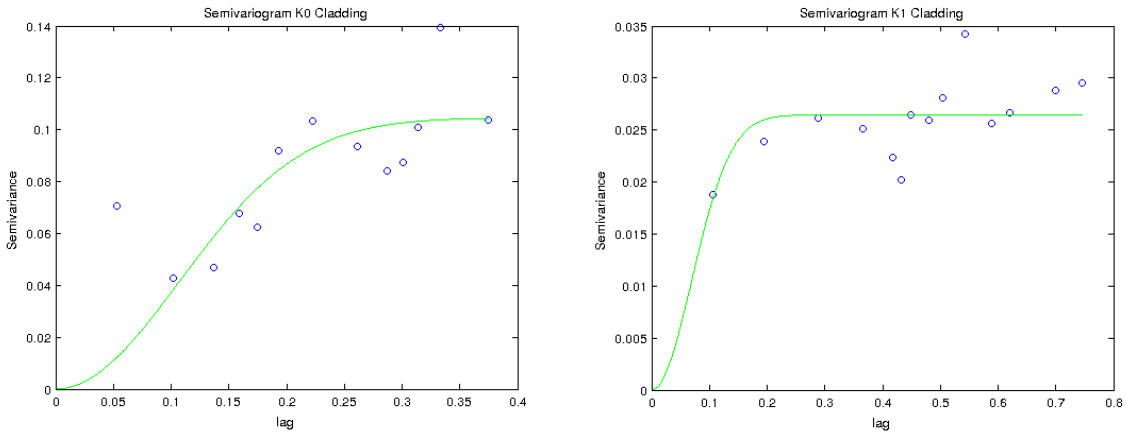

Figure 3.3.2: Semivariograms for Each of the Cladding SIFICs

It is shown in the figures above that each of the semivariograms was approximated using the continuous Gaussian function represented by the plotted line. The resulting semivariogram plots show that the base coefficients were modeled more effectively than the cladding SIFICs. This is likely due to the fact that the cladding dataset is twice as large, as each SIFIC is determined as a function of two cladding thicknesses in addition to the other terms.

In the event that this method is selected to be used in the final implementation of the research goals, which have previously been described, a more accurate representation of the cladding semivariograms may be necessary. As it was stated before, these functions are difficult to approximate in closed form, and thus the data can, at times, be scattered in relation to the closed form expression.

The form of each semivariogram was selected using Matlab's non-linear least squares polynomial fit function. However, for each of the semivariograms, the number of bins and range of lags considered for each of the forms was not selected in a mathematically rigorous manner. Thus the forms of the models shown above likely have room for improvement.

3.4 Surrogate Model Comparison

In this section, each of the surrogate modeling techniques previously discussed was applied using FAVOR's existing SIFIC data. However, before using the surrogate models in an actual flaw analysis, it would be useful to develop a method for comparing all the modeling techniques. Both interpolation and kriging models will always reproduce the exact output when evaluated at one of the points included in the calibration data, while it is likely that a response surface will not. As stated in section 3.2.1, even though RSM does not accurately predict all of the calibration points, it can still be very good at predicting unknown points, which is the purpose of the model. Therefore, in order to conduct a comparative study between each of the three modeling techniques and their ability to predict unknown data, the following procedure was utilized.

For each of the four models, one data point was randomly selected to be withheld from the dataset. The four surrogates were then created using the smaller dataset, and used to predict the withheld input. The corresponding SIFIC output for each of the four surrogates was then compared to the actual value provided by FAVOR. This process was then repeated a 100 times for the base SIFICs and 200 times for the cladding SIFICs. A rough convergence study was conducted in order to determine the number of appropriate samples. As the existing datasets are relatively small for the base and cladding SIFICs (189 and 378 respectively) 100 and 200 respective samples proved to be adequate.

After finding the predicted SIFIC for each of the surrogate models, the absolute difference between the actual and predicted value for each of the four surrogates was found and converted to a percentage error. The tables below represent the mean error percentage for each of the surrogate types, as well as the standard deviation of the corresponding 100 or

200 error percentage values.

	Mean Error Percentage Value					
Model	K0	K1	K2	K3	K0_cl	K1_cl
Interp.	1.69	5.60	8.60	24.01	14.42	11.88
Cubic RS	3.23	3.58	5.23	8.01	23.22	20.88
Quad RS	1.45	2.13	3.76	6.51	92.60	55.77
Kriging	2.17	10.62	10.92	40.10	48.31	28.86
	Standard Deviation of Error Percentage					
Model	K0	K1	K2	K3	K0_cl	K1_cl
Interp.	2.23	8.21	10.73	51.72	40.25	18.11
Cubic RS	4.45	4.79	7.22	11.07	59.30	19.13
Quad RS	1.19	2.12	4.25	7.11	558.57	269.63
Kriging	3.00	36.63	17.53	96.06	268.21	62.68

Table 3.4.1: Raw Error Percentages and Std. Deviations

The results in table 3.4.1 show that for each of the modeling techniques, it becomes more difficult to accurately predict the value of the SIFIC as the order of said value increases. Additionally, the cladding coefficients in general were more difficult to accurately predict than those for the base metal. An acceptable level of error for each of the models would be less than roughly ten percent, so many of these are far too large to implement.

However, upon analyzing the outputs, most values were consistent with the actual FAVOR SIFIC values. The prevailing issue with these meta-models is their inability to extrapolate outside of the design space. As such, if the randomly selected point to be excluded and analyzed happens to fall near the edges of the supplied data, the metamodel is forced to extrapolate, and the resulting output can be wildly inaccurate. Thus, a small percentage of extreme values can drive up the mean error percentage, which is what is shown in Table 3.4.1. In future studies to generate the SIFICs for 3D flaw orientations, a wide range

of parameter values will need to be sampled to ensure that the metamodels will not be required to extrapolate beyond the bounds of the model.

In order to combat the issue of extrapolated data in the above data set, the extrapolated values were removed from each of the surrogate models to represent their predictive abilities in a fully realized design space. Table 3.4.2 shows the results of the same study with the extrapolated values removed.

	Mean Error Percentage Value					
Model	K0	K1	K2	K3	K0_cl	K1_cl
Interp.	0.78	2.19	4.21	6.67	4.26	4.33
Cubic RS	1.43	1.64	2.38	3.94	13.98	13.49
Quad RS	1.01	1.29	1.92	3.61	13.14	13.61
Kriging	0.96	2.14	3.30	7.90	8.04	12.08
	Standard Deviation of Error Percentage					
Model	K0	K1	K2	K3	K0_cl	K1_cl
Interp.	0.77	2.64	5.06	6.97	10.83	10.85
Cubic RS	1.18	1.34	1.86	2.62	7.61	8.48
Quad RS	0.63	0.82	1.62	2.69	7.11	8.02
Kriging	0.97	2.59	5.09	11.23	9.45	10.94

Table 3.4.2: Adjusted Error Percentages and Std. Deviations

As shown in Table 3.4.2, after the extrapolated values are removed from the dataset, each of the models show a fairly significant increase in overall accuracy. The interpolation method appears to represent the cladding coefficients somewhat more effectively than the other methods. This result is due to the fact that only two discrete values of the cladding thickness were provided in the table. As such, given the method of randomly selecting a point to exclude from the model calibration set, the excluded point always occurred at one of the two discrete values, meaning that no interpolation was required between cladding

thickness values. Table 3.4.2 shows that all of the methods are relatively equal in their ability to represent the base coefficients.

Chapter 4. Final Framework

In the preceding chapters of this thesis, various techniques for analyzing surface breaking flaws in RPVs have been discussed, where specifically, the application of the weight function method, described in Section 2.1, is of particular interest. Although this method has been implemented successfully within the FAVOR code, its limited analysis to axis aligned flaws for primarily discrete flaw characteristic inputs demonstrates the potential for model improvements to be made.

The process of implementing the weight function method was described in Section 2.2, where it was shown that the method has essentially two major components required to obtain a solution. The first component is a set of coefficients describing the stresses in the crack-free RPV wall, obtained in the global RPV finite element model, and the second is the creation and selection of the appropriate SIFICs. Although throughout this thesis, the proposed methodology for individually accomplishing each of these tasks has been discussed, the final framework, combining each of these components for use in probabilistic analyses, has not. As such, the following chapter will begin with a high level overview of the planned implementation, where specifics of the final analysis framework will be presented. As this is massive undertaking, there are components of the framework that have yet to be fully developed and implemented. Thus, a discussion of the current implementation as well as preliminary results of its application will then be covered, followed by an overview of the current framework's applicability to the proposed framework, as well as a summary of the future plans.

4.1 Proposed Framework

In order to combine all of the elements previously described in this thesis into a single

cohesive analysis, RAVEN can be used. RAVEN is a risk assessment code currently under development at the Idaho National Lab capable of driving Grizzly, or other MOOSE based applications, in various types of statistical analyses. Specifically, RAVEN can be used to alter parameters within Grizzly model input files in a statistical or directly specified manner such that models can be analyzed parametrically. RAVEN is also capable of creating surrogate models using a database of input and output data. Additionally, reduced order model forms can be developed or specified using data within RAVEN, and can then be used for repeated evaluation in probabilistic analyses.

For the goals of this project, RAVEN can be useful in a number of ways, the most significant of which is its ability interact with and drive Grizzly FEA models. In other words, Grizzly model inputs can be controlled explicitly or statistically using RAVEN, where the resulting outputs can be accessed for further steps in the analysis. Thus, in the proposed final implementation, RAVEN will be used as the modeling framework combining each the Grizzly model components necessary of the weight function method for probabilistic risk assessments. Specifically, in the final implementation proposed, RAVEN's role in the project will be as follows: First, it will be used to drive Grizzly sub-models for the creation of the SIFIC database. The resulting SIFICs will then be stored in RAVEN where it will, using one of the techniques discussed in Chapter 3, create a surrogate model capable of predicting the appropriate SIFICs as a function of any continuous flaw characteristic input. RAVEN will also drive Grizzly's evaluation of the global finite element model, where the results will be combined with predicted SIFICs, using the methods described in Section 2.2.2, to form the deterministic model. RAVEN will then be used to evaluate the deterministic model in a probabilistic assessment, where any type of flaw or transient can be considered.

4.2 Framework – RAVEN Implementation

The full implementation of RAVEN and Grizzly, as specifically outlined above, is an ongoing research effort involving both the INL and ORNL. Additionally, both Grizzly and RAVEN codes are relatively new, where some of the required capabilities are still being developed. Thus, several of the requirements mentioned above cannot yet be implemented, the details of which will be presented in this section. Early RAVEN implementation work has focused primarily on driving Grizzly sub-models to create the library of SIFICs.

The process of automating both the creation and evaluation of flaw sub-models is made difficult due largely to the fact that each model requires its own unique mesh. It is relatively simple to automate the process of applying different boundary conditions and evaluating each model, but mesh generation is generally a problem dependent issue relying heavily upon model geometry. For Grizzly analyses, the mesh generation is generally performed using an external application, the most common of which is program called Cubit. Cubit is a command based 3D mesh generation software capable of being scripted using variables and logic. Cubit is therefore particularly useful in automating meshing processes, and was thus the mesh generation software used in this work. Sub-model meshing scripts were then created such that the flaw characteristics were defined as variables that were subsequently used to shape the mesh. Additionally, an interface between Cubit and RAVEN was created such that pre-determined sets of variables could be changed within the cubit meshing script using RAVEN. A RAVEN input was then created which interfaced with both Cubit and Grizzly in order to create and evaluate sub-models for a range of flaw characteristics. Though the initial database was relatively small, it demonstrated that RAVEN is capable of driving the development of an SIFIC database.

After RAVEN was used to drive the creation and evaluation of the Grizzly crack sub-models, a number of issues regarding the RAVEN framework and Grizzly sub-model results were made apparent. The first was a compatibility issue, where stress intensity factor outputs from Grizzly could not be used by RAVEN. This essentially meant that the library of SIFICs could be created using RAVEN and Grizzly as intended, but after that, could not be accessed by RAVEN for surrogate model formulation. This is an issue that is currently being addressed by members of the RAVEN development team. Additionally, as shown in Figure 2.3.9, inconsistencies between the Abaqus and Grizzly SIFICs were found. The inconsistencies were found during a convergence study on mesh and sub-model domain size effect, where it was determined that those factors were not the cause of the discrepancy. Although the source of error has yet to be fully identified, it is currently being addressed by the Grizzly development team. These issues involve critical components in the structure of the overall analysis and thus, the implementation of RAVEN as the analysis framework was temporarily suspended.

4.3 Framework – Matlab Implementation

As it was just made clear that RAVEN would be unable to access the SIFICs found from the Grizzly sub-models, the analysis was instead driven using Matlab. Additionally, as it had just been shown that the Grizzly sub-model results were not entirely consistent with FAVOR's existing library of Abaqus solutions, the FAVOR library of SIFIC data was used. These adjustments were made in a general way, such that the principles demonstrated in Chapters 2-3 could be applied to a real problem, demonstrating proof of concept, for eventual use within the proposed framework.

In order to demonstrate the validity in the application of each of the methods and

concepts previously described in this thesis, the following analysis was performed. Using FAVOR's FAVLOAD module, and separately, the Grizzly code, the global RPV response to the PTS event shown in Figure 2.3.1 was found. The results from FAVLOAD were then used in FAVOR's FAVPFM module where a single deterministic analysis was performed resulting in a time dependent stress intensity factor. Similarly, the global finite element model shown in Figure 2.3.2 was evaluated using Grizzly, where the normal stresses in the vessel wall were obtained. Then, using each of the 4 surrogate models described in Chapter 3, the values for the SIFICs were determined and combined using FAVOR's methodology, detailed in Section 2.2.2, in order to demonstrate each surrogate modeling approach (though only one is required for the analysis). The result: four stress intensity factors, each obtained using the same global model results, however, different SIFIC approximation techniques. The results from each of the five models are shown below in Figures 4.3.1 and 4.3.2. Figure 4.3.2 is a closer view of the peak stress intensity factor shown in Figure 4.3.1. The flaw depth used in the analyses was specified as .865 inches, corresponding to a depth relative to wall thickness of 10%. Although only one flaw sample is shown, these results are representative of the many cases evaluated during the course of the comparison.

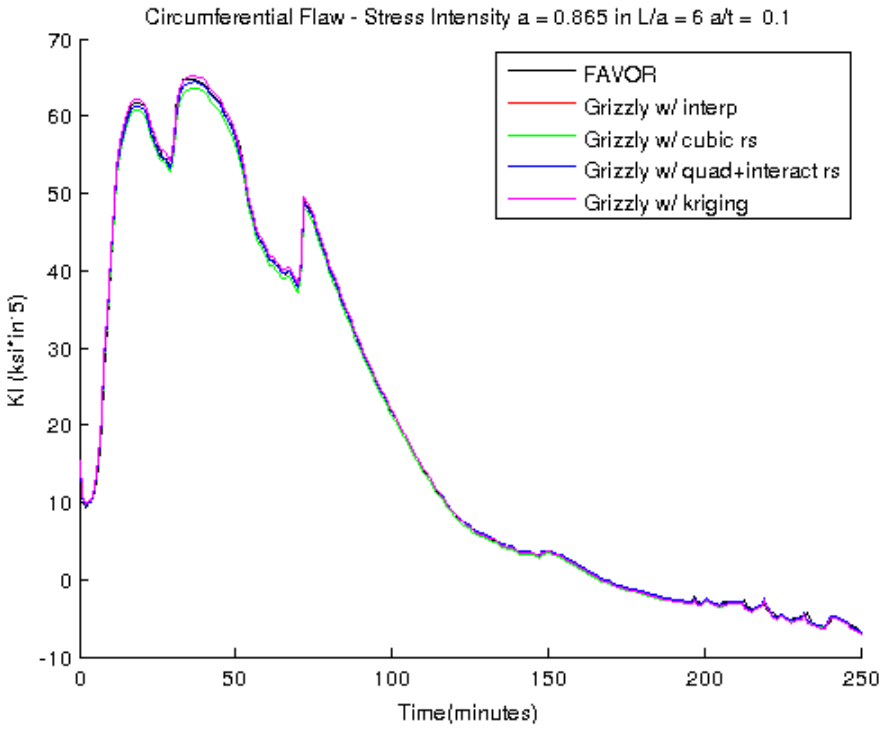

Figure 4.3.1: FAVOR Grizzly Surrogate Model Comparison

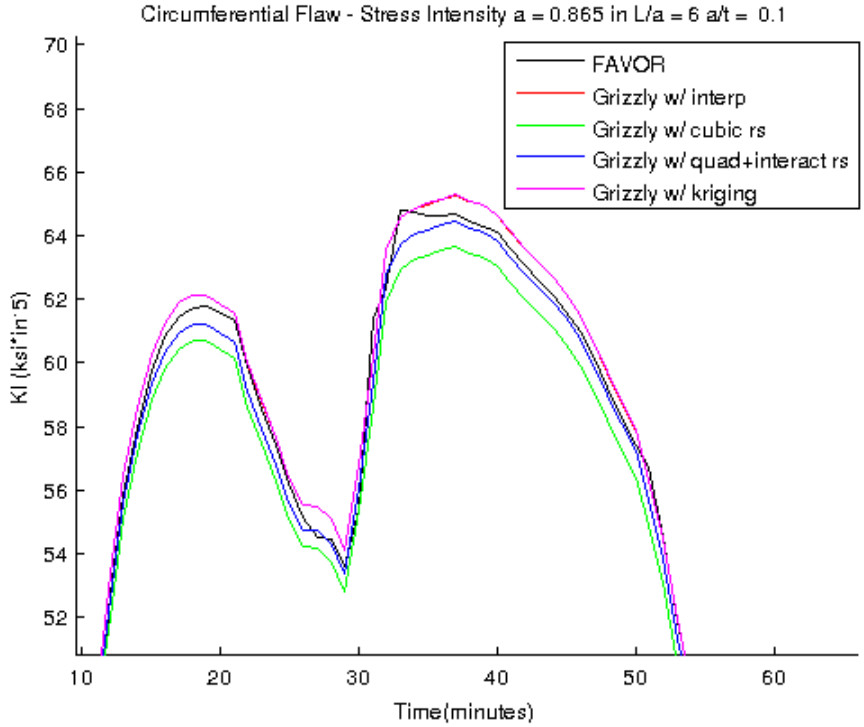

Figure 4.3.2: FAVOR Grizzly Surrogate Model Comparison

The results shown in the figures above illustrate very good agreement between FAVOR and the each of the Grizzly models using surrogate modeling for SIFIC approximation. The comparison above shows that each of the surrogate modeling techniques is valid for SIFIC approximation, and that Grizzly can be used to effectively measure the global RPV's thermomechanical response during a simulated pressurized thermal shock event. Though these concepts were not demonstrated through the use of RAVEN, as directed in the project goals, the implementation using Matlab is easily transferrable to the desired framework.

It was also demonstrated that RAVEN is capable of driving Grizzly sub-models to create a library of SIFICs, though issues within the Grizzly code resulted in disagreement with the validated solutions. Additionally, capabilities within RAVEN are currently under development such that the output database can be used in the surrogate model formulation. When the issues within RAVEN and Grizzly are resolved, the methods verified in the study conducted above can be implemented fully within the desired RAVEN framework for use in a probabilistic assessment.

As the eventual goal of this work is to develop a more general capability for evaluating a wider variety of flaw geometries, it is important to explore the possibility of utilizing surrogate modeling techniques. Future project plans would require a larger database of SIFICs where the values are dependent on additional input parameters. As the dimensionality of interpolation increases, so does the number of required data points for accurate representation. With kriging or RSM, this increased cost may not be as pronounced, allowing a potential savings in simulation time required to populate the SIFIC tables and an increased accuracy in their predictive capabilities. Furthermore, due to the probabilistic

output of the kriging approach, the uncertainty (potential error) that exists in the surrogate model's prediction of an unknown flaw geometry's SIFIC values can be determined and potentially propagated through the probabilistic analysis.

Chapter 5. Summary

Throughout this thesis, methods for approximating the stress intensity factor of surface breaking elliptical flaws in reactor pressure vessels have been presented, analyzed and applied. This is an ongoing research effort, where the primary goal is to perform computationally efficient probabilistic risk assessments on embrittled RPVs containing some arbitrary distribution of flaws in a simulated pressurized thermal shock event. Models currently in use are limited to flaws aligned with the central axes of the RPV. Thus, the range of considered flaws can be expanded to enable more thorough analyses. In order to accomplish this, the goal of this research was to investigate the possibility of extending the current analysis methods to an environment that enables the evaluation of 3D off axis flaws.

The first step in this process included a review of the current methods used, as well their implementation in existing models. Thus, in Chapter 2, a well-established, widely used method for approximating the stress intensity factor of a flaw was introduced. This method is used within the Fracture Analysis of Vessels (FAVOR) code as a deterministic reduced order model for rapid evaluation in probabilistic analyses. FAVOR's procedure was shown to require two components: the coefficients describing a cubic polynomial fit to stresses in the crack free RPV wall, and a set of pre-determined stress intensity factor influence coefficients corresponding to the geometry of the flaw being analyzed. In order to procure each of these elements, the INL's Grizzly code was used.

Grizzly was chosen as the finite element analysis tool because of its ability to model material aging and embrittlement as well as fracture mechanics and thermomechanical transient processes. Therefore, in accordance with the analysis techniques described in Chapter 2, a finite element model was created representing the crack-free RPV wall. This

model was then exposed to time dependent temperature and pressure boundary conditions, simulating a pressurized thermal shock event. The resulting stresses and temperatures obtained from the Grizzly RPV model were found to be consistent with validated FAVOR solutions, and could thus be implemented in the final RPV analysis. In addition to the global RPV model, RPV crack sub-models were then created in an effort to re-create a library of SIFICs for future analyses. Although many of these sub-models were created and evaluated using Grizzly, inconsistencies with validated Abaqus solutions were identified. Differences between the two solution sets identified a likely source of error within the Grizzly code that is currently being addressed by the development team. Thus, Grizzly sub-model results were not used for the final application in this project, and for further steps in this analysis, FAVOR's existing library of SIFICs was utilized.

After evaluating Grizzly models and determining a source for each of the required solution method's components, a potential limitation was illustrated within the current analysis method. Specifically, in Section 2.2, it was shown that current analyses within FAVOR can vary flaw depths as continuous values, but all other flaw characteristics required as inputs to the model must be discrete values corresponding to exact SIFIC data. To enable any continuous input within the domain of data would allow for more thorough analyses at minimal costs in terms of computation. Additionally, in the event that these methods are extended to 3D off axis flaws, a broader database of SIFICs will be required such that additional flaw characteristics can be represented. For those reasons, various forms of surrogate modeling were presented and applied in Chapter 3 to determine their validity as a surrogate for the actual SIFIC database. It was shown in Sections 3.4 and 4.2 that any of the methods outlined in Chapter 3 could be used in order to accurately predict SIFICs.

Furthermore, the use of surrogate models enables the analysis of any continuous flaw characteristic, provided that the supplied characteristic values are contained within the range of model calibration data.

After demonstrating the validity of the surrogate models for use in SIFIC approximations, the final task of the project was to demonstrate each component in a full deterministic analysis. In the project's final implementation, each of the components previously described will be conducted using the INL's RAVEN code. RAVEN is a statistical analysis tool capable of driving Grizzly FEA models, creating reduced order models, and conducting Monte Carlo simulations for probabilistic analyses. Thus the implementation of the methods described above using RAVEN began. Using RAVEN to drive Grizzly sub-models, the ability to create a library of SIFICs was demonstrated. However, issues within the RAVEN/Grizzly interface prevented its use in further analyses. Additionally, as previously mentioned, the SIFICs produced within Grizzly have yet to be validated, and thus were also excluded from the final analysis.

For the reasons explained above, the application of the methods covered in this thesis were performed using Grizzly for the global RPV analysis, FAVOR's existing library of SIFICs, and surrogate models created in Matlab. These elements were combined using Matlab in a process consistent with the FAVOR analysis, outlined in Section 2.2. The results are shown in Section 4.2 and were found to be consistent with the FAVOR solution.

It is important to identify that although Grizzly sub-model results are currently not valid, the existing models developed throughout this research can be used to provide accurate results when issues within the Grizzly code are resolved. Additionally, their implementation within the desired RAVEN framework can be accomplished when issues within the

RAVEN/Grizzly interface are resolved. The surrogate modeling techniques presented in this work are existing capabilities within the RAVEN framework. As they have now been shown to be valid approximation methods, their usage within RAVEN can be quickly implemented once the issues in the code are resolved by the development team.

References

[1] G. E. Lucas, G. R. Odette, "Embrittlement of nuclear reactor pressure vessels," *The Journal of The Minerals, Metals & Materials Society,* Volume 53, Issue 7, pp. 18-22, July, 2001.

[2] R.L. Klueh, A. T. Nelson, "Ferritic/martensitic steels for next-generation reactors," *Journal of Nuclear Materials,* Volume 371, Issues 1–3, pp. 37-52, 15 September 2007.

[3] Cheverton et al., "Behavior of Surface Flaws in Reactor Pressure Vessels Under Thermal-Shock Conditions," *Experimental Mechanics,* Volume 21, Issue 4, pp. 155, 1981.

[4] M. E. Riley, W. M. Hoffman, "Risk Analysis of Reactor Pressure Vessels Considering Modeling-Induced Uncertainties," *Journal of Verification, Validation, and Uncertainty Quantification,* Under Review, 2016.

[5] Dickson et al., "Grizzly/FAVOR Interface Report," Oak Ridge National Lab, Oak Ridge, TN, 2013.

[6] R. Kryter, "Integrated assessment of pressurized thermal shock," (NUREG/CP--0041-Vol6), United States, 1983.

[7] H. F. Bückner, "A Novel Principle for the Computation of Stress Intensity Factors," *Z. angew. Math. Mech. 50,* pp. 529-546, 1970.

[8] Stephens et al., Metal Fatigue in Engineering, Wiley-Interscience, 2001.

[9] F. Simonen, "A Generalized Procedure for Generating Flaw Related Inputs for the FAVOR Code," NUREG/CR-6817, Rev. 1.

[10] M. N. Guian Qian, "Procedures, Methods and Computer Codes for the Probabilistic Assessment of Reactor Pressure Vessels Subjected to Pressurized Thermal Shocks," *Nuclear Engineering and Design, Volume 258,* pp. 35-50, May 2013.

[11] Williams et al., "Fracture Analysis of Vessels – Oak Ridge FAVOR, v12.1, Computer Code: Theory and Implementation of Algorithms, Methods, and Correlations," ORNL/TM-2012/567, USNRC Adams number ML13008A015, Oak Ridge, TN, 2012.

[12] Dickson et al., "Stress-Intensity-Factor Influence Coefficients for Axial and Circumferential Flaws in Reactor Pressure Vessels," in *ASME Pressure Vessels and Piping Conference*, 1993.

[13] Spencer et al., "Reactor pressure vessel integrity assessments with the Grizzly simulation code," in *SMiRT-23*, Manchester, UK, August 10–14, 2015.

[14] "50 Years of Nuclear Energy," International Atomic Energy Agency, 2008.

[15] Busby et al., "Materials Degradation in Light Water Reactors: Life After 60," ORNL/TM-2008/170, Oak Ridge, TN, 2008.

[16] Bryson et al., "Stress-Intensity-Factor Influence Coefficients for Circumferentially Oriented Semielliptical Inner Surface Flaws in Clad Pressure Vessels (Ri / t = 10)," ORNL/NRC/LTR-94/8, Oak Ridge National Laboratory, Oak Ridge, TN, 1994.

[17] R. J. Schmidt, A. P. Boresi, Advanced Mechanics of Materials, Wiley & Sons , 202.

[18] J. R. Rice, "A path independent integral and the approximate analysis of strain concentration by notches and cracks," *Journal of Applied Mechanics,* pp. 352-379, 1968.

[19] Spencer et al., "3D J-Integral Capability in Grizzly," Light Water Reactor Sustainability Program, Idaho National Lab, Idaho Falls, ID, September, 2014.

[20] Jin et al., "Comparative studies of metamodelling techniques under multiple modelling criteria," *Structural and Multidisciplinary Optimization,* Vol. 23, no. 1, pp. 1-13, 2001.

[21] G. E. P. Box, K. B. Wilson, "On the Experimental Attainment of Optimum Conditions," *Journal of Royal Statistics Society,* Vol. 13, Series B, pp. 1-45., 1951.

[22] T. G. Sitharam, P. Samui, "Application of Geostatistical Models for Estimating Spatial Variability of Rock Depth," *Scientific Research,* vol. 3, pp. 886-894, 2011.

[23] M. L. Stein, Interpolation of Spatial Data: Some Theory for Kriging, New York: Springer Science, 1999.

[24] N. Cressie, "The Origins of Kriging," *Mathematical Geology,* Vol. 22 , no. Issue 3, pp. 239-252 , 1990.

[25] S. H. Ahmadi, A. Sedghamiz "Application and Evaluation of Kriging and Cokriging Methods on Groundwater Depth Mapping," *Environment Monitoring and Assessment ,* Vol. 138 , no. 1-3, pp. 357-368, 2008.

[26] Zimmerman et al., "A Comparison of Spatial Semivariogram Estimators and Corresponding Ordinary Kriging Predictors," *Technometrics, 33(1),* pp. 77–91, 1991.

[27] G. M. Laslett, "Kriging and Splines: An Empirical Comparison of their Predictive Performance in Some Applications," *Journal of the American Statistical Association,* Vol. 89, no. 426, pp. 391-400, 1994.

[28] Sacks et al., "Design and analysis of computer experiments," *Statistical Science,* pp. 409-423, 1989.